ISBN 978-82-326-6869-4 (printed ver.)
ISBN 978-82-326-6163-3 (electronic ver.)
ISSN 1503-8181 (printed ver.)
ISSN 2703-8084 (electronic ver.)

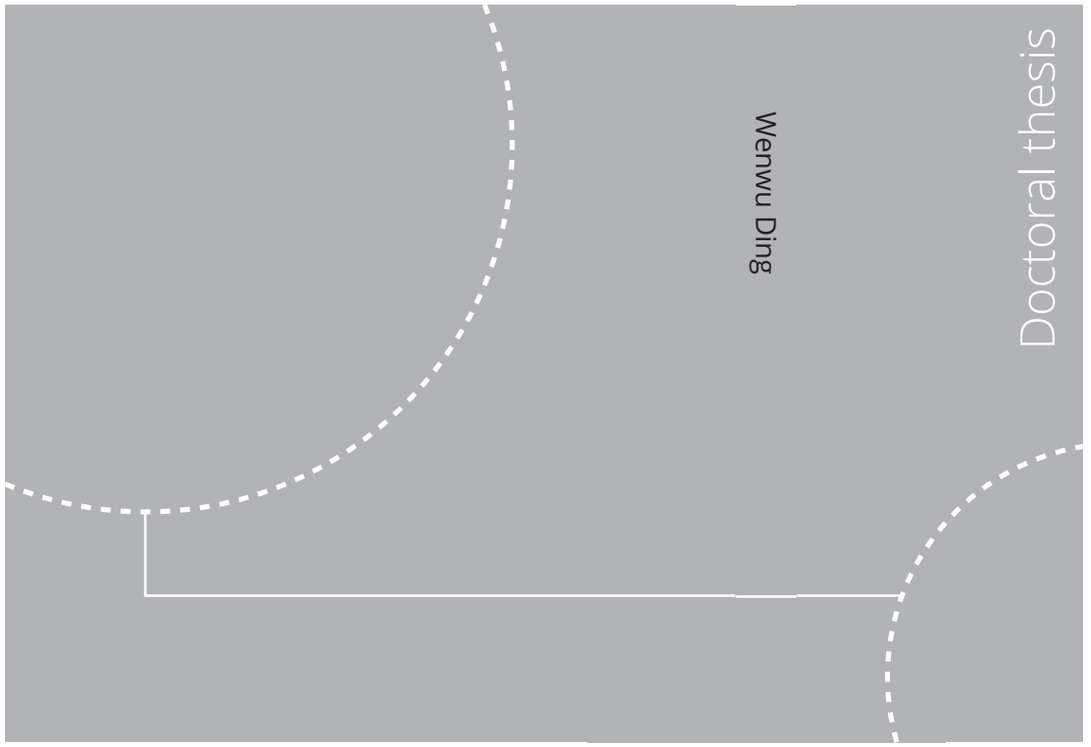

Doctoral theses at NTNU, 2021:235

Wenwu Ding

Conical micro-structures for super-repellent surfaces and their effect on droplet impact

NTNU
Norwegian University of
Science and Technology

Doctoral theses at NTNU, 2021:235

NTNU
Norwegian University of
Science and Technology
Thesis for the degree of
Philosophiae Doctor
Faculty of Engineering
Department of Energy and Process Engineering

NTNU
Norwegian University of
Science and Technology

Wenwu Ding

Conical micro-structures for super-repellent surfaces and their effect on droplet impact

Thesis for the degree of Philosophiae Doctor

Trondheim, July 2021

Norwegian University of Science and Technology
Faculty of Engineering
Department of Energy and Process Engineering

NTNU
Norwegian University of
Science and Technology

NTNU
Norwegian University of Science and Technology

Thesis for the degree of Philosophiae Doctor

Faculty of Engineering
Department of Energy and Process Engineering

ISBN 978-82-326-6869-4 (printed ver.)
ISBN 978-82-326-6163-3 (electronic ver.)
ISSN 1503-8181 (printed ver.)
ISSN 2703-8084 (electronic ver.)

Doctoral theses at NTNU, 2021:235

Printed by Skipnes Kommunikasjon AS

Abstract

Surface wetting properties control is crucial to various applications, such as anti-wetting, self cleaning and heat transfer processes. Design of surface wetting properties can be achieved by mechanical and chemical methods. The mechanical methods include surface roughness design, while chemical methods involve changing the intrinsic wetting properties of the surface. The intrinsic wetting properties, which can be characterized by the contact angle on a flat surface, can reach a maximum of 120°. The combination of roughness and chemical treatment can distinctly enlarge the contact angle range, including wicking (zero contact angle), partial wetting (finite contact angle) and superhydrophobicity (contact angle larger than 150°). Thus, a lot of works showing various types of structure design with different wettability properties can be found in the literature.

Among the various possible micro-structures, conical structures (well-known structures found in the Lotus leaf) are frequently used due to their unique properties. The Lotus leaf has a lot of micro-scale tapered bumps and also nano-scale roughness. Various previous works artificially produce this kind of conical structures and achieve similar wetting properties. However, a lot of these works use non-regular conical like structures, while the number of works using patterned conical structured surfaces is limited. Therefore, it remains unclear how the different conical geometries can affect the wetting properties of the surface. To bridge this gap, we fabricate patterned conical micro-structured surfaces with different cones geometry and topography and study how the static and dynamic wetting properties are affected by the structures. The conical micro-structures are produced on silicon substrates using photo-lithography and plasma etching techniques. By varying the fabrication process recipe, different types of conical structures are fabricated. This thesis presents the study of both static and dynamic wetting properties for various conical structured surfaces. In addition, cylindrical pillar structured surfaces are also used for comparison.

It is found that the conical structured surface can be designed to be super-repellent for intrinsic contact angles larger than 90°. The conical half-apex angle of the cones is important for suppressing the Cassie-Wenzel transition. This work not only provides more insights into the effect of conical structures on wetting but also shows that conical structures can be a good path for achieving superhydrophobicity.

In addition to the previous study of Cassie wetting state on conical structures, we subsequently investigate how the partial wetting Wenzel droplet shape is affected by the conical pillars sidewall geometry. We compare truncated cone pillars with cylindrical pillar surfaces. Previous works show that pillar height/pitch can affect the liquid droplet final shape. However, we observe that the drop shape on truncated cones and on cylindrical pillars is different even when they have the same pitch and height. Besides, the drop shape on these two types of surfaces is also evolving in a different way as the impact Weber number increases. This work reveals that the micro-structures side wall topography can influence the final drop shape.

We further investigate conical structures as a means to increase the anti-wetting properties of surfaces during impact of low surface tension droplets. We fabricate conical pillars surfaces with re-entrant like side wall roughness all along the side

wall, which looks like a tree-branch topography. Low surface tension drop impact experiments are conducted on these surfaces and we show that the tree-branch like structure does improve the anti-wetting performance by exhibiting a higher critical Weber number (the Weber number starting to show partial rebound), compared with conical structures without a sidewall roughness. The tree-branch like structures can reduce the solid-liquid contact and have higher resistance to penetration, and thus can reach higher anti-wetting performance than other reported rigid surfaces.

Finally, we explore how conical and cylindrical pillar structures behave for water droplets impacting at different Weber numbers. We show how the liquid residue size is affected when the droplet impacts above the critical Weber number for conical and cylindrical pillars. It is shown that the conical pillar surfaces have higher contact angle and lower hysteresis while the cylindrical pillars show lower contact angle and higher hysteresis for dense array surfaces. At low Weber number, conical structures surfaces show less energy dissipation compared with cylindrical structures surfaces. For the same height and pitch, the cylindrical pillars show a higher critical Weber number compared with conical pillars due to the large solid-liquid contact at the pillar top. However, the liquid residue when the Weber number is above the critical Weber number for the cylindrical case is larger than for the conical pillar case. We propose that the liquid residue size is affected by the We number, anti-penetration ability and liquid mobility inside the structures. Liquid mobility within the conical structures is lower than for the cylindrical ones, which leads to less wetted area due to less open space inside the structures.

This work not only reveals how the conical geometry can affect the wetting properties but also shows that conical structured surfaces are a good candidate for anti-wetting performance enhancement, which can be useful for various applications.

Acknowledgements

The thesis work is partially done at Thermal Two-Phase Flow Laboratory from Department of Energy and Process Engineering, and partially done at NTNU Nanolab. The various structured surfaces are produced at Nanolab and characterized also there. Thanks a lot for the generous help from Nanolab engineer, just name a few, Svenn Ove Linde, Mark Giulio Chiappa. In addition, thanks a lot to my colleague Espen Rogstad, who helps me a lot for photo-lithography and plasma etching work. In addition, I sincerely thanks Reidar Tellebon for helping me to build the experiment set-up. Further, I am deeply grateful to Professor Maria Fernandino and Professor Carlos Alberto Dorao for providing me the position and also supervising my PhD work here. You are nice supervisor who can not only help in the lab but also help in publication work. With your help, I can have solid progress in my PhD work.

Besides, I want to express my thanks to my colleagues, Wenjing, Han, Manuel, Marcel, Jonas, Damiano, Julian, Diego, Ernest, Subhanker, Suparna, Xiongjiang, Yue, Gonzalo, Keunsoo, Il Woong, Jeongrim, with your care and help, I can finally get out of the difficult period and get rid of the frustrations. In addition, I want to thanks my landlord Egil, not only a landlord but also a nice friend. Living in your place is full of care and fun.

Finally, I want to express my gratitude to my family, my father and my mother have raised me up and always support me, thus I can have the opportunity to initiate and finish the PhD work. Last, I want to gratefully acknowledge Haoran, you have provided me a lot care and support during my PhD life, best wishes for you!

Wenwu Ding

World Peace!

Contents

Chapter 1

Introduction

1.1 Background and motivation

Droplet wetting phenomena are not only widely observed in nature but also fundamental to various industry processes [1]. Various applications are related with droplet wetting properties, for example, self-cleaning surfaces [2, 3, 4, 5], inkjet printing [6, 7, 8, 9], liquid metal printing [10, 11], solder droplet printing [12, 13], microfluidics [14, 15, 16], chemical shielding [17, 18, 19], antifouling [20, 21], anti-fogging [22, 23, 24] and anti-icing surfaces [25, 26], dropwise condensation [27, 28, 29, 30, 31] and evaporation [32, 33, 34].

In nature we find various wetting phenomena. For example, a rain drop sitting on a Lotus leaf displays superhydrophobic conditions, which can be a good way to achieve anti-wetting applications like self-cleaning, antifouling, antifogging and anti-icing [36, 35]. Rice leaf [37, 38] and butterfly wing [39, 40] display anisotropic wetting properties which promote directional droplet movement, thus it is useful for applications like microfluidics and condensation. Desert beetles [41] survive in arid environment with different wettability patterns on their back, which collect water efficiently. Hence it unveils strategies for applications like water collection and condensation process. For an extensive review the reader is referred to [35]. Figure 1-1 shows four types of special wetting observed from nature [35].

Lessons from natural plants or animals pave the way for artificial fabrication of

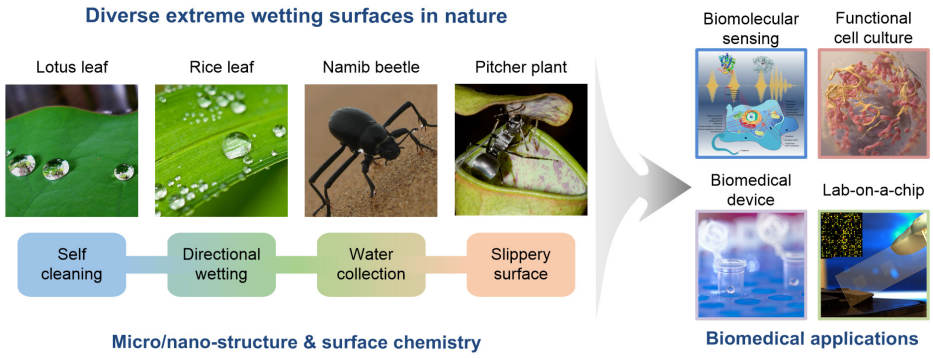

Figure 1-1: Nature can provide solutions for special wetting properties, reprinted from [35].

surfaces with different wetting properties. By chemical coating, structure design or both combined, various functional surfaces are produced with desired wetting properties [1, 35]. However, when it comes to the control of wetting properties, better design guidelines are still needed. With more and more new reports, the knowledge gap is being reduced. Unfortunately, the physics behind are still lacking in some fields. For instance, the role of contact line and contact area on contact angle is under debate [42], the wetting dynamics around the contact line [43] is illusive, the role of different forces at different scales on droplet wetting/dewetting dynamics is still unclear [44] especially for complex fluids, and the role of the structures sidewall topography also remains to be investigated.

Superhydrophobic surfaces display excellent anti-wetting properties. It is observed that the micro-nano tapered structures on the Lotus leaf makes the leaf superhydrophobic and thus rain drops roll off the surface easily [36]. The structure of the Lotus leaf is shown in Figure 1-2. In addition to natural conical-like structures, there are also artificially fabricated conical-like structures [45, 46, 47, 48, 49, 50] showing similar anti-wetting performance. Either on natural or artificial conical-like structures, high contact angle and low adhesion properties are shown, which could be a potential way to achieve better self-cleaning performance. Moreover, the liquid on cones exhibits directional movement [51, 52, 53, 54, 47, 55], which therefore benefits

applications like condensation/water collection [56, 57, 58]. However, the role of conical microstructures and their topography on wetting properties remains unclear. In short, the unique properties of cones and the associated applications propel further development and research in this regard.

This thesis considers surfaces with conical structures and investigates how they can improve the anti-wetting properties of a surface. To mimic the tapered structures and study the associated wetting properties, we choose to produce conical structures and investigate their wetting properties. Natural structures are randomly distributed as shown in Figure 1-2 and thus the distance between the structures, structures height and structures sidewall shape can be different on the same surface. This kind of irregular pattern hinders the investigation of tapered structures geometry on the surface wetting properties. Therefore, we fabricate patterned conical structures with a defined geometry to take the study in this field forward.

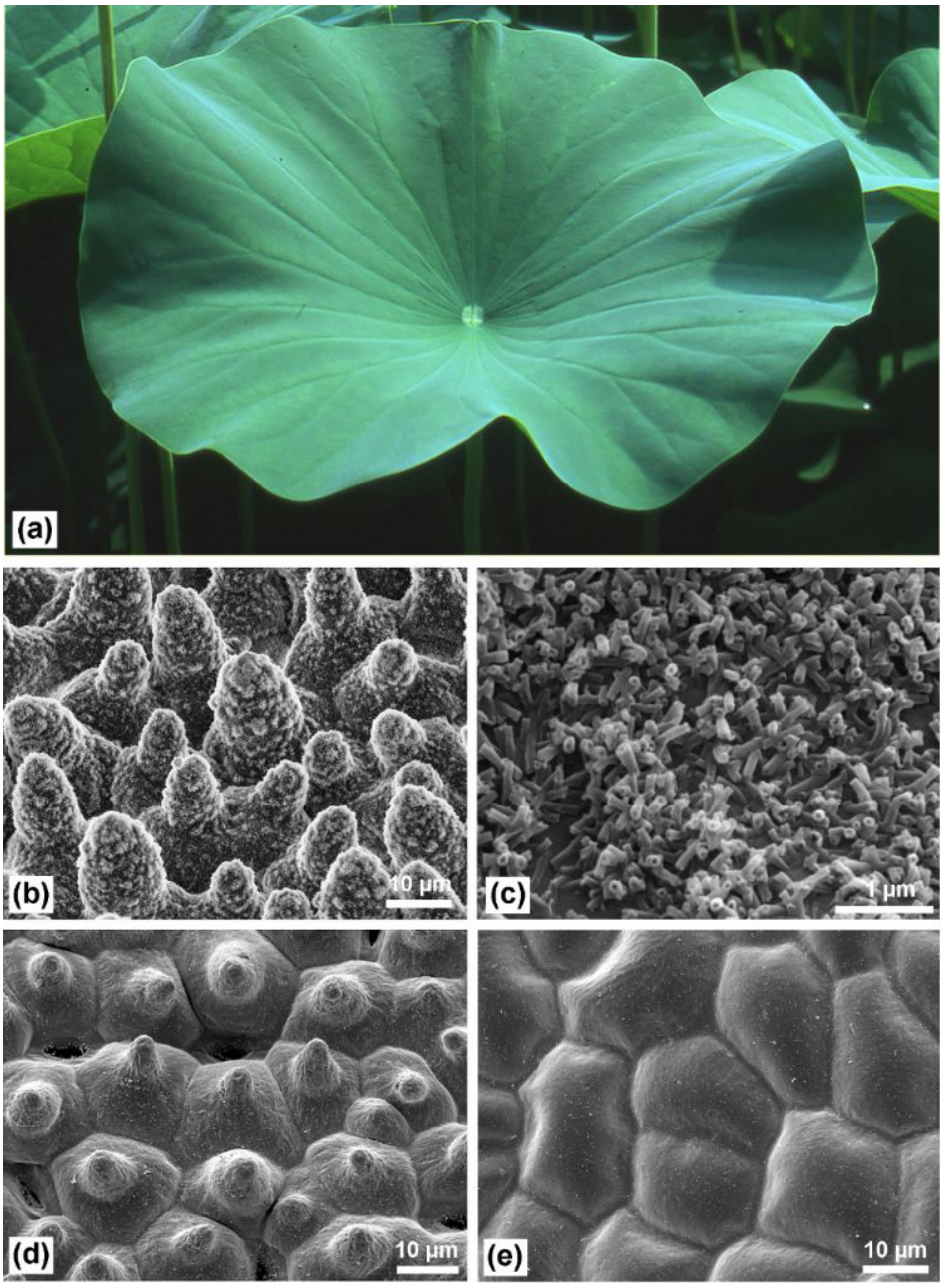

Figure 1-2: Self cleaning lotus leaf and its structure, tapered bumps are observed from scanning electron microscope images, reprinted from [36].

1.2 Goal and objectives

The main goal of this work is to study the effect of conical microstructures and their topography on surface static and dynamic wetting properties.

The objectives are:

- Investigate the effect of conical structured surfaces on wetting properties during Cassie wetting state conditions (apparent contact angle, contact angle hysteresis, superhydrophobicy and low adhesion)
- Investigate the effect of conical structured surfaces on Wenzel state droplet shape.
- Study of droplet impact behavior for different conical structured surfaces, both for water and low surface tension fluids, to increase the anti-wetting performance and reveal the associated physical mechanism.

1.3 Scope

The work here is focused on experimental investigation. The samples produced are silicon based flat or structured surfaces. Structured surfaces include truncated conical structured surfaces, conical structured surface and cylindrical pillar surfaces. Wetting properties like contact angle and contact angle hysteresis and droplet impact dynamics are investigated at ambient conditions, using de-ionized water or ethanol-water mixture as the liquid phase.

1.4 Structure of the thesis

The thesis has 7 chapters and the main contents of the different chapters are listed below.

- Chapter 1: Presents the research background, motivation, research goal and objectives, research scope, theory and state-of-the-art.

- Chapter 2: Presents details of the samples fabrication procedure and experimental set-up.

- Chapter 3: Study of the effect of conical micro-structures on static water drop wetting properties in Cassie-Baxter state.

- Chapter 4: Study of the effect of structure sidewall and droplet impact inertia on Wenzel drop shape.

- Chapter 5: Study of drop impact dynamics on various conical structured surfaces for low surface tension fluids.

- Chapter 6: Study of water drop impact dynamics on conical structured surfaces and cylindrical pillar surfaces.

- Chapter 7: Summary and future work.

1.5 Theory and state-of-the-art

Depending on the wetting properties of the solid surface, a water droplet exhibits different curvature, which is normally described by a parameter called contact angle. The contact angle is defined as the angle between the triple line tangent and horizontal axis, which is used as a way to quantify the wetting properties of the surface. Based on the contact angle, four wetting cases are observed, namely superhyhyophilic case (hemi-wicking/wicking with 0° contact angle), hydrophilic case (contact angle from 0° and below 90°), hydrophobic case (contact angle larger than 90°), superhydrophobic case (contact angle larger than 150°). Contact angle hysteresis is frequently used as a way to quantify surface adhesion properties, which is defined as the difference between advancing angle and receding angle. In a tilting experiment, the advancing angle is the front side contact angle when the liquid front starts to advance and the receding angle is the rear side contact angle when the liquid starts to recede.

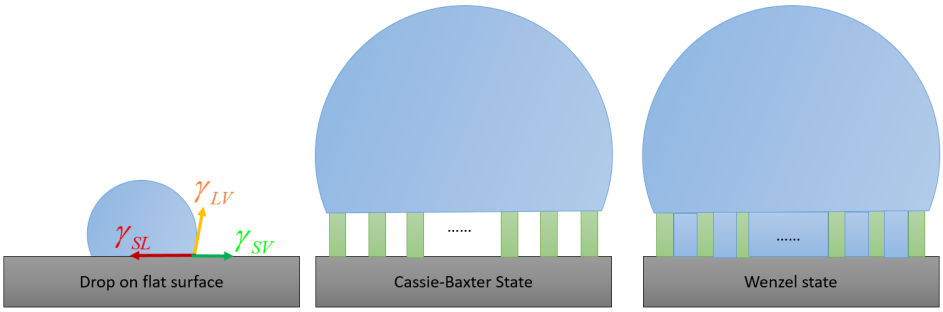

Figure 1-3: Schematic representation of a drop on a flat surface and a structured surface. For the latter case, Cassie-Baxter state and Wenzel states are shown. In reality, a drop on a structured surface could also show a mixed state.

1.5.1 Static wetting on flat surfaces

On an ideal flat, homogeneous solid surface, a liquid drop displays certain contact angle θ_Y, which can be described by Young's equation [59] written as

$$\cos\theta_Y = \frac{\gamma_{SV} - \gamma_{SL}}{\gamma_{LV}} \tag{1.1}$$

This well-known equation describes the force balance at the triple line per unit length. The solid-vapour surface tension γ_{SV}, solid-liquid surface tension γ_{SL} and liquid-vapour surface tension γ_{LV} reach an equilibrium condition with γ_{LV} showing a macroscopic contact angle θ_Y.

1.5.2 Static wetting on structured surfaces

The ideal case is described by Young's equation, but the surface in reality is not ideal. The surface can be chemically heterogeneous or contain random/patterned micro/nano structures. On a structured surface, the macroscopic contact angle is related with the microscopic solid-liquid interaction. Two cases are frequently studied, Wenzel state and Cassie-Baxter state.

In Wenzel state, the liquid penetrates into the structure at the microscopic level and the intrinsic wetting properties will always be enhanced. Intrinsic hydrophilic

surfaces will be more hydrophilic, and the intrinsic hydrophobic surfaces will become more hydrophobic. The roughness factor r is used to describe to what extent the wettability is enhanced, which is defined as the ratio of actual solid-liquid area to the projected solid-liquid area. This equation is written as

$$\cos\theta_W = r\cos\theta_Y \tag{1.2}$$

Different from the Wenzel state, the Cassie-Baxter state [60] is normally a hydrophobic condition with liquid sitting on top of the surface roughness. In this case, the cosine of the apparent contact angle is a weighted ratio between $\cos\theta_Y$ on the solid part and the air part ($\cos\theta_{air}$= -1 for air), written as

$$\cos\theta_{CB} = f_1\cos\theta_Y - f_2 \tag{1.3}$$

The angle θ_{CB} is the apparent contact angle, f_1 is the actual solid-liquid contact fraction, f_2 is the air part fraction. The θ_Y is the equilibrium contact angle on the flat surface. There is still debate about the role of droplet contact area and contact perimeter in predicting the apparent contact angle [42]. Here we use area fraction in calculating f_1 and f_2, where f_1 is the solid-liquid contact area divided by the projected area, and f_2 is the liquid-air contact area divided by the projected area.

Control of wetting is crucial to various applications, therefore predicting the wetting state has been studied previously in several works [61, 62, 63]. For applications requiring superhydrophobic conditions, Cassie-Baxter state is needed. However, Wenzel state is preferred for applications demanding larger solid-liquid contact. The equilibrium state can be estimated by comparing the energy state between these two wetting states. The surface energy includes terms from solid-liquid interface, solid-vapour interface and liquid-vapour interface. Thus, a critical contact angle [61, 62, 63] is used when the Cassie state and Wenzel state are equal in energy variation, which is obtained by equating equation (1.2) and equation (1.3) as

$$\cos\theta_C = -f_2/\left(r - f_1\right) \tag{1.4}$$

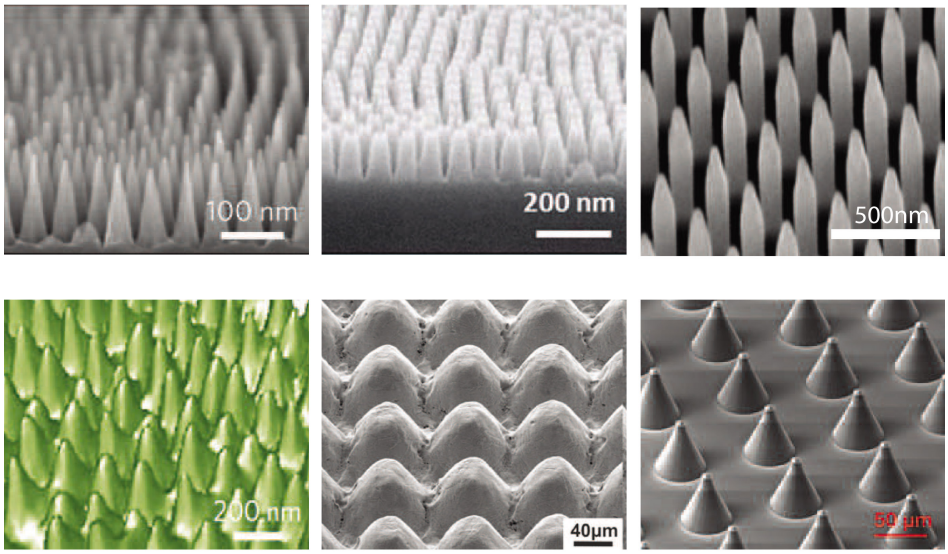

Figure 1-4: Conical structures reported in previous work [45, 46, 47, 48, 49, 50]. The different scales of the conical structures can all show high contact angle, as summarized in [64].

The angle θ_C denotes this critical contact angle. For a given structure and θ_Y, the Cassie-Baxter state is favored if the θ_Y is larger than the θ_C, while on the contrary Wenzel state is favored.

Li et al.'s work [63] has revealed that spontaneous Wenzel to Cassie transition is achieved when the structure design is in mono-stable Cassie state (when the critical contact angle is smaller than receding contact angle on the same flat surface). In reality, there exist extra factors, for example triple-line pinning, which can violate the critical contact angle analysis. Cassie-Baxter state could be observed even though Wenzel state is the lower energy state compared with Cassie state, which is due to the extra pinning resulting in higher energy barrier. Therefore extra energy input is needed to overcome the barrier.

As mentioned above, the structure design can affect the wetting state distinctly. A large number of surfaces [65] have been reported to achieve superhydrophobic states, such as carbon nanotubes [66], re-entrant structures [67] and multi-re-entrant hier-

archical structures [68], macro-micro roughness structures [69] and conical structures [70, 71, 72, 47]. In particular, conical micro- and nano-structures have been observed to show a high contact angle and low hysteresis, for example the cicadae wings covered by conical protuberances [73] or fabricated surfaces with cone-like structures [45, 46, 47, 48, 49, 50], as shown in Figure 1-4. Tapered conical structures reduce the top solid-liquid contact and pinning effect [74, 64], hence they pave a good pathway for anti-wetting structure design. In addition, the conical design parameters range from nanometer scale to micrometer scale but all display higher anti-wetting properties in the literature. However, the governing physics for showing high contact angle (in the range around 160°-180° [45, 46, 47, 48, 49, 50]) is not clear. In Chapter 3, we further the research in this part by revealing the dominant factor behind the high contact angle of conical structured surfaces.

1.5.3 Heterogeneous shape of Wenzel state droplet

A droplet normally adopts a spherical shape from a top view on a flat homogeneous surface. Non-spherical shapes can be obtained by structure design or chemical heterogeneity design. Manipulation of the shape is especially useful to various printing applications, like inkjet printing [6, 7, 8, 9], liquid metal printing [10, 11], solder droplet printing [12, 13]. Therefore it is essential to have better understanding of how the droplet shape is influenced by the different liquid dynamics. In numerous works, droplet profiles imaged from the side view are presented for Wenzel state surfaces, but not all works record the top view image. Previous works have showed that the drop shape from a top view can be heterogeneous. Various shapes are formed, which is closely related with the pattern design parameters.

Various drop shapes are observed depending on the conditions of the surface and droplet itself. It is well-known that surfaces patterned with different wettability coating manage to create different shapes [75], since chemical heterogeneity would pin the droplet as the designed shape. On non-isotropic structures, droplet shapes are distinct heterogeneous, for example the groove type structure [76, 77, 78, 79, 80, 81], where the droplet shape parallel to the grooves is different from the one

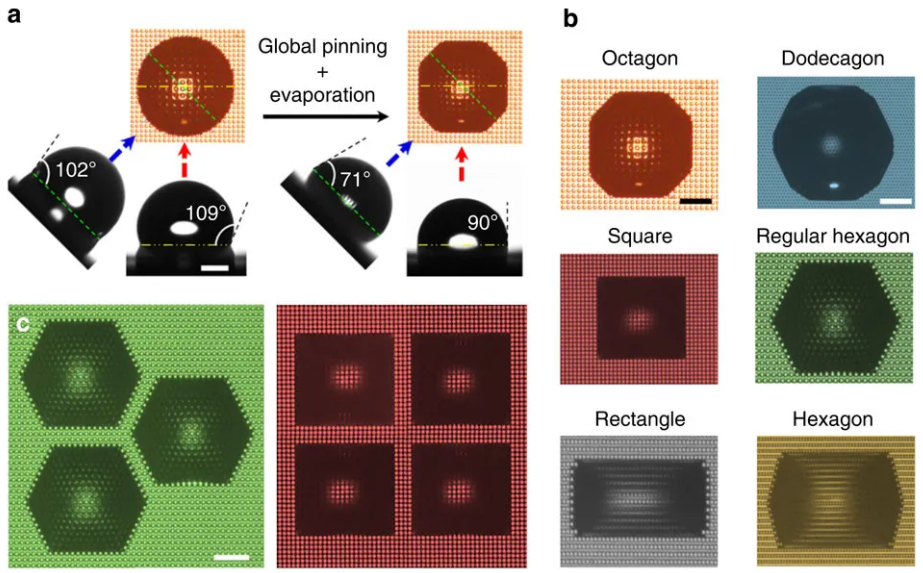

Figure 1-5: Heterogeneous shape on various structured surfaces, reproduced from [75].

perpendicular to grooves. Free energy and energy barrier models are used to explain this heterogeneity [76, 77, 78, 79, 80, 81]. The drop final shape is estimated by minimizing the free energy [76]. However the equilibrium condition is related with the number of structures below the liquid. Additionally, due to the difference in energy barrier for the liquid to move in different directions, the drop would form various shapes. The free energy models mentioned above use equilibrium angle or define a dynamic contact angle, which needs to be adjusted for dynamic processes far from equilibrium where the apparent contact angle is affected by the contact line moving velocity [43]. The free energy based model needs to be further developed by considering contact line dynamics.

Isotropic structures also affect the wetting shape [82, 83, 75]. The factors reported to affect the drop shape include pattern size [82], structure design parameter like height/pitch [83], drop surface tension [83], symmetry and spacing of pillar lattice [84], diameter/pitch [75] and concentration of mixture [85, 86]. In addition to

free energy and energy barrier models, the physics behind the various factors are mainly ascribed to how liquid evolves during the spreading process [83, 87, 88, 75]. The heterogeneity in shape is described by the different spreading velocities at the horizontal direction (parallel to square structure array) and diagonal direction [83] (diagonal to the square structure array). The velocity is a result from the associated forces, namely, capillary and viscous forces [83]. Chen et al.'s work has shown that the droplet shape heterogeneity is affected by the excess driving force and resistance force induced by micropillars [87]. Apart from the previous two forces, pinning force is also mentioned to play a role [89, 83, 84]. Raj et al.'s work [75] proposes the advancing contact angle model, which revealed that the various shapes are due to the different wetting advancing angles at the horizontal and diagonal directions with respect to the square structure array.

From the above literature survey, it is shown that both energy based models (free energy and energy barrier models) and force based models (capillary force, viscous force, pinning force) are used to analyze the Wenzel drop shape heterogeneity. The energy model is based on the minimization of the system free energy and thus predicts the droplet shape at meta-stable and equilibrium states [76]. Though this model is suitable for analysing droplet shape at both non-equilibrium and equilibrium conditions, the resulting shape is affected by the initial input setting. For example, the number of pillars below the droplet could affect the final shape [76], droplet dynamics are affected by input of apparent contact angle or slip coefficient [90], or the way to deal with the contact line [91, 92]. Additionally, liquid on curved surfaces like cones exhibits asymmetric local liquid contact line profile [55] which is not equilibrium condition and influences the solid-liquid interaction. The non-monotonous variation of dynamic apparent contact angle with contact line velocity [43] further dictates extra effort in modelling of the droplet dynamics.

The force model describes the local force at the contact line thus it describes both the equilibrium and dynamic condition. When all the associated forces are well established, the liquid spreading velocity can be estimated and thus the shape is estimated. For example, the capillary and viscous force model estimates spreading

well [93] in the wicking range. But in the finite contact angle range, the capillary and viscous force model fails as extra forces exist. For example, when pinning force is distinct, the droplet contact line is pinned locally and thus the droplet stays in non-equilibrium state [89, 83, 84]. In addition, inertia force plays a distinct role [94], but there is a lack of such inertia effect study for patterned structured surfaces. Moreover, liquid flow differences below and above the structures top exist [95, 96], thus the drop shape is a result of combined effects from the two spreading processes. At the inertia-capillary regime, the drop shape would be altered due to the difference of liquid flow above and inside the structures. However, it is difficult to isolate the contribution of different forces, therefore it remains unclear how the drop shape is governed in the finite contact angle range. We advance this part in Chapter 4 by studying the role of inertia force for patterned structured surfaces.

Among the various forces, the change of structure parameters would result in a change of capillary force, viscous force and also pinning force. Previous works have reported the effect of different structure design parameters on the drop final shape but the effect of structure lateral wall shape is lacking. In the literature, groove side wall shapes [81] are shown to play a role in the shape heterogeneity but the role of the pillar side wall shape is not studied. The change of structure lateral wall shape is expected to influence the force terms and thus affect the drop shape. In Chapter 4, we contribute in this area by investigating experimentally the role of the pillar lateral wall topography on the droplet shape.

1.5.4 Wetting behavior during drop impact

Drop impact outcome and surface properties

When a drop impacts onto a solid surface, different impact outcomes are observed for smooth or structured surfaces. In both cases, the outcome can be complete rebound/deposition, partial rebound, receding break-up or splashing when Weber number (this dimensionless number is used to describe the rebound condition, $We = \frac{\rho R V^2}{\gamma}$, ρ is density, V is impact velocity, γ is surface tension, both droplet radius R and diameter D appear in literature as characteristic length, R is used in this work) is increased

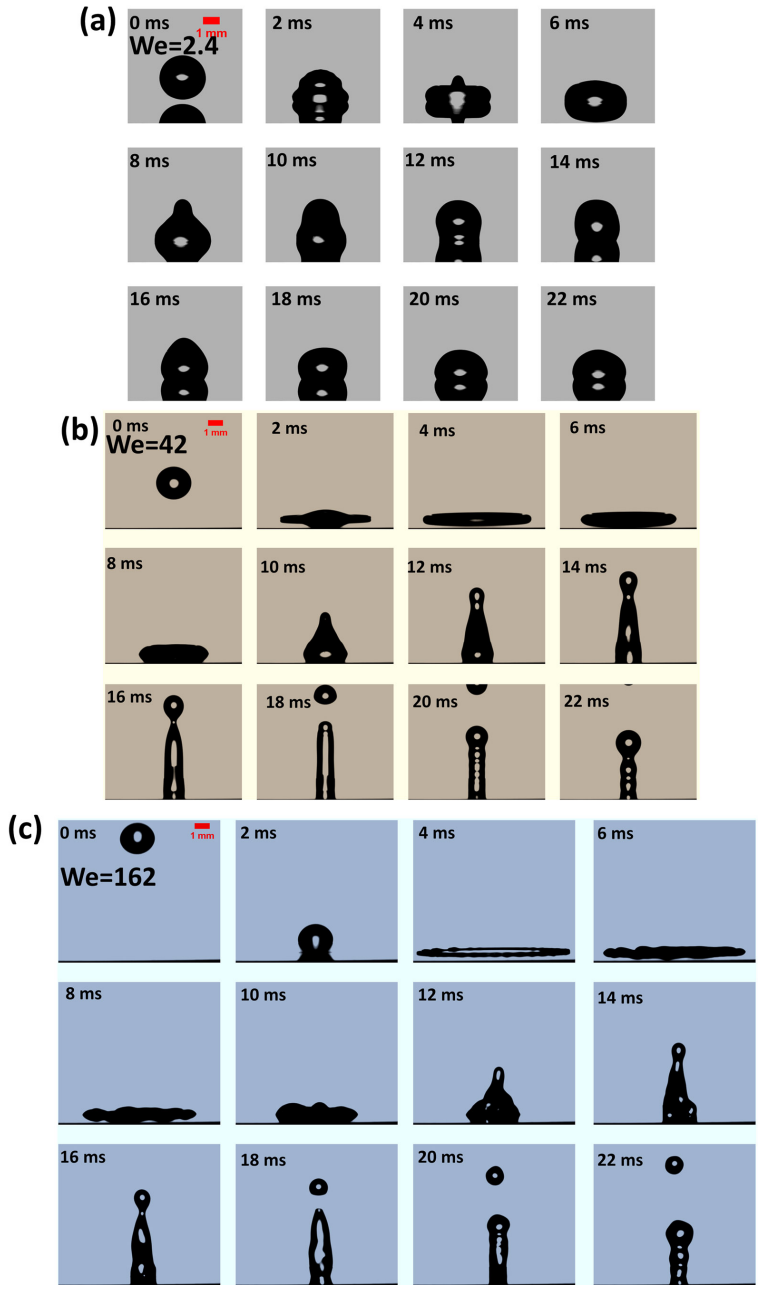

Figure 1-6: Water drop impact on flat hydrophobic silicon surface. At We=2.4, the impact is in deposition regime. At We=42 and We=162, the impact regime is partial rebound. The surface has a contact angle of 107° for water droplet.

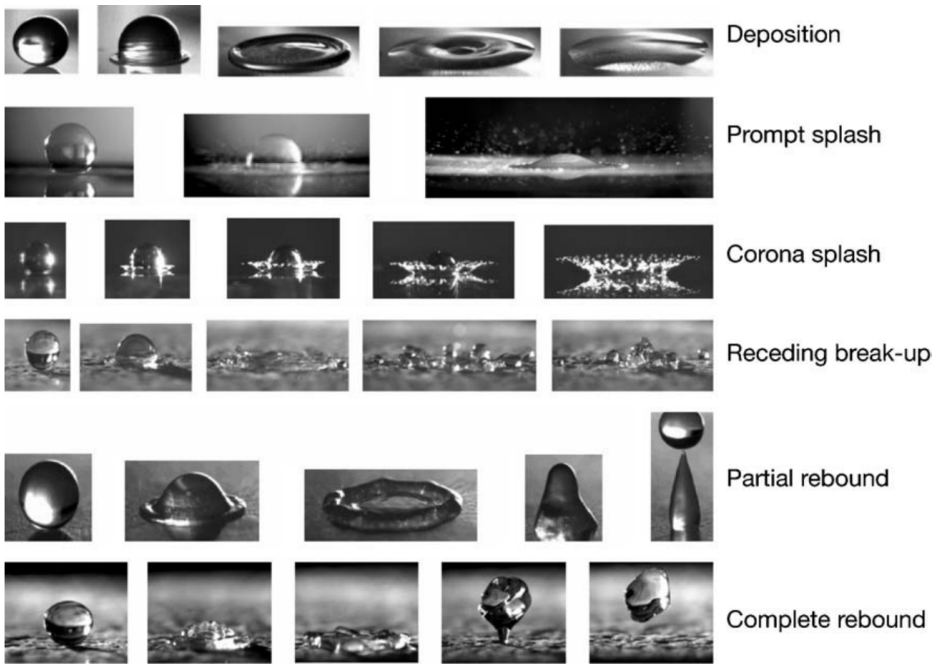

Figure 1-7: Impact regime images from Yarin's work [97].

[98, 99, 97, 100]. Typical impact outcomes are shown in Figure 1-6 for smooth case and Figure 1-7 for structured surface.

In Figure 1-6 (a), selected images of a water drop impact are presented when depositing a drop on a flat surface with contact angle of 107°. Three impact conditions are presented here. At small Weber number of 2.4, deposition regime is observed. The droplet undergoes deformation in spreading and retracting process and sits still after some oscillations. At increased We number, the liquid drop will spread to larger contact baseline size, as displayed in Figure 1-6 (b) and (c). Partial rebound is observed at We=42 and We=162 on this smooth surface. Complete rebound also happens on smooth surfaces but it only appears in the small velocity case with narrow velocity range due to the air film existence below the droplet [101]. In this work, complete rebound for smooth surface is not observed in the test range, as shown in Figure 1-6.

Figure 1-7 shows more impact outcomes. At deposition case (first line of Figure 1-7), the droplet stays on the surface without rebound due to high energy dissipation. Prompt splash (second line of Figure 1-7) case displays small detached droplets at the liquid lamella front when impacting on the rough surface at higher We number. Corona splash (third line of Figure 1-7) happens when reducing surface tension and differs from prompt splash by showing rising liquid lamella. The liquid lamella of receding break-up case (fourth line of Figure 1-7) breaks into several fingers due to capillary instability [97]. Partial rebound (fifth line of Figure 1-7) occurs on the rough surface by showing liquid residue pinned on a surface, while complete rebound (last line of Figure 1-7) is observed on the rough surface where the whole droplet leaves the surface.

The solid-liquid contact is more complex for structured surfaces. Figure 1-8 (reprinted from [102]) displays the dimensionless contact baseline (contact baseline divided by initial droplet diameter) with time for three wettability cases at We=3.9 [102] on smooth surfaces. This plot shows that the dimensionless contact baseline in the advancing stage falls on a similar curve while the dimensionless contact baseline in the receding stage deviates for these three cases [102, 103]. However, the

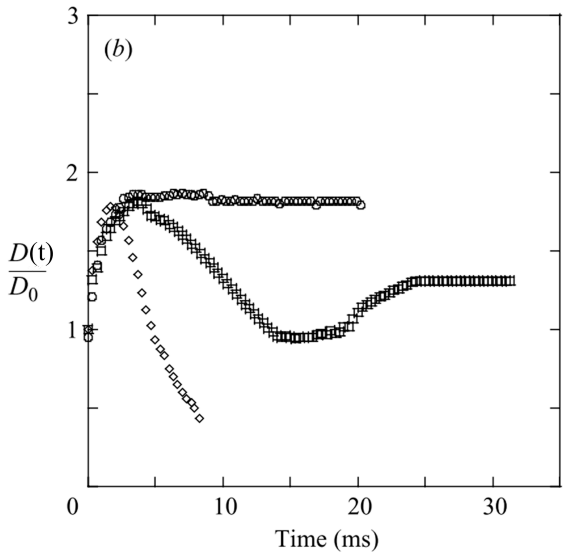

Figure 1-8: Dimensionless contact baseline (contact baseline divided by initial droplet diameter) reprinted from [102] for water drop impact at We=3.9 with different wettability on flat surface.

dimensionless contact baseline for different contact angle cases collapses onto similar curve during the receding stage for structured surface in the literature [104]. On certain structured surfaces, especially superhydrophobic ones, the liquid can recede to zero solid-liquid contact not only at low Weber number case [101] but also at higher We number condition [97]. The surface wetting properties determine whether there is complete rebound and also how many times the bouncing would happen. It has been shown that the dynamic contact angle influences the drop impact behavior [105, 106, 107, 108], as the advancing/receding angle affects liquid movement during the advancing/receding stage especially, which further results in energy dissipation difference between different dynamic contact angle cases. Additionally, the wetting dynamics are altered when the substrate molecular composition is changed though the equilibrium contact angle is fixed [92]. The type of roughness structure also affects the impact outcome, which is closely related with the liquid penetration [109, 110] and local wetting properties. Besides, it is shown that hierarchical structured surfaces

promote splashing compared with smooth surfaces, micro structured surfaces or nano structured surfaces [99]. In short, the We number, wettability and roughness all play a role in the drop impact process.

From an energy balance perspective, the different drop impact outcomes are closely related with energy transfer difference. During the drop impact process, the energy balance includes kinetic energy, surface energy, energy dissipation due to viscosity and gravitational potential energy [111]. Gravity effect is usually not considered as an important term for drop impact phenomena [97], thus the gravitational potential energy part is not considered here during the contact process. The droplet at first spreads, which is driven by kinetic energy. The kinetic energy is transformed into surface energy and partly lost in viscous dissipation. After maximum spreading, the droplet starts to recede, where the surface energy stored in droplet deformation drives the receding. In this stage, part of the surface energy is converted to kinetic energy, and part lost in viscous dissipation. However, energy dissipation at the contact line is shown to affect drop impact dynamics as well [112, 113, 114, 115, 116, 117, 44, 118]. In addition to viscous dissipation [119, 120] in the liquid, the energy dissipation in the air film for low We number cases has been shown to affect the dynamics as well [101]. After take-off, the droplet energy during air flight not only converts to gravitational potential energy but also converts to oscillatory kinetic energy [121, 122]. In a non-wetting situation, the effect of viscosity is ignored [123] especially when using low viscosity liquids. Viscosity of air is also quite small. Therefore viscosity dissipation during the air flight stage is ignored here.

As shown in Figure 1-7, the deposition regime shows no bouncing and the partial rebound regime displays liquid residue pinning on the surface, which is against the anti-wetting purpose. In the literature, the criteria for having a rebound include that droplet energy (initial energy - dissipation energy) just before rebound should be larger than a certain droplet energy threshold [119], exceeding the corresponding receding diameter [120], the receding angle has to be larger than certain value or saying hysteresis has to be smaller than certain value [105, 106]. Three cases when a droplet does not rebound or partially rebounds are:

1) deposition regime. At very low Weber number, the regime is called deposition, which shows no bouncing as the kinetic energy is too low [97, 124]. In this case, the droplet is not bouncing due to limited impact energy compared with energy dissipation (viscous dissipation and energy dissipation at the contact line). However, the deposition regime is not observed for our superhydrophobic surfaces in the current work;

2) partial rebound. With increasing impact velocity, droplet bouncing back leaves part of the liquid behind on the solid surface [97], where part of the liquid transits to the partial Wenzel or Wenzel state at the impact center;

3) full Wenzel state at high We number. Droplets behave like in the deposition regime [125] with full droplet no-bouncing, which is due to high adhesion at Wenzel state.

The second and third categories both exhibit no bouncing, stemming from increased solid-liquid contact which results in distinct energy dissipation (viscous dissipation and energy dissipation at the contact line). In general, the energy dissipation has to be minimised in order to have a rebound.

Surrounding gas and air film

It is reported that the surrounding gas properties can affect the drop impact dynamics. For instance, the decreasing of surrounding gas pressure can suppress splashing [126]. When reducing the air density, the splashing is attenuated [127] as well. The splashing liquid is found to spread on a thin air film rather than initial solid-liquid contact [128]. An impacting drop on a solid surface could be deformed as a dimple due to increased air pressure below the drop before actual contact with the surface [129, 130, 131, 132, 133, 134]. The air film lubricates the drop producing a skating like effect, which breaks via spinodal-like mechanism [131]. The existence of an air film can produce wettability independent bouncing [101].

The evolution of the air film has been visualized by x-ray imaging [132] and high-speed colour interferometry [133]. The air dimple height is related with the impact velocity [135] and structure [133]. A micro structured surface has larger dimple height than a smooth surface [133], where it is proposed that the extra structure creates

additional pressure build-up due to more resistance for air flow. They also show that bigger and denser structure leads to larger dimple height. Though an air film is widely observed at the initial stage of the drop impact, the air film would be entrapped as a bubble and the liquid contact the structure. It is reported that the liquid penetrates into the micro structure around the central bubble region [136] at higher We number and more wetted area is shown with higher pitch design. They [136] also display that directional splashing is related with the lattice arrangement, but it is suppressed by reducing the air pressure resulting in less liquid surfing on air, thus decreasing the spreading lamella size. On nano-rough surfaces, the central air disk is also observed during drop impact with a band of micro-bubbles forming around the central air disk [137], where the micro-bubble formation is affected by the impact velocity, roughness and wettability. In addition to the bubble entrapment during the initial spreading mentioned above, Chen et al.'s work [138] reports bubble entrapment, which is formed during recoiling when the existing cylindrical air cavity is stretched due to asymmetric retraction and finally collapse. This type of bubble entrapment happens only in certain We number-contact angle range.

Increasing surface bouncing ability

Though an initial air film exists on smooth or structured surfaces, the air film is entrapped as a bubble around the impacting center when the droplet approaches the surface. Additionally, the gas inside the structure could be squeezed out when the liquid penetrates the structure, for instance, due to intrinsic wetting or due to high impact velocity [109, 110]. It is reported that [109, 110] Cassie-Wenzel transition happens when the impacting velocity lies above a threshold velocity for structured surfaces, which leads to distinct energy dissipation and results in partial rebound or non-bouncing full Wenzel state droplet. In order to have less energy dissipation during droplet impact, the design of the structures should reduce the solid-liquid contact area with more gas cushion below, thus less viscous energy dissipation [109] or energy dissipation at the contact line would occur.

From the gas properties perspective, increasing the gas viscosity is able to increase the flow resistance which would help to preserve the gas cushion. However, in most

applications, the gas phase is not under manipulation. In this work, the gas phase is also fixed to be air. Hence design of the structures is usually used as a strategy. To reduce the gas depletion, design of the structures on a surface would help either by increasing the gas flow resistance or improving the anti-penetration ability.

Firstly, the gas flow resistance could be increased to avoid gas drainage. By using denser or larger pillars, the gas flow resistance is increased resulting in more air film [133]. The flow resistance is further increased by downscaling of the structures, as the flow resistance is larger using multiple small channels compared with fewer larger channels with the same total flow cross section area [133]. Therefore, nano structures normally have higher flow resistance compared with micro structures. It is also reported that hollow pillar structures show better anti-wetting performance during drop impact, as the non-communicating structures keep more air below the droplet [139]. In addition, hierarchical structures introduce extra roughness, which in theory also increase the flow resistance.

Secondly, the liquid penetration should be avoided using proper structure design. A dense array of structures would help to reduce liquid penetration [109, 140, 141, 142, 110, 143], where the capillary force or pinning force is larger to resist penetration. Furthermore, nano structures (downscaling of the structures) increase the anti-wetting capillary pressure thus the liquid has more difficulty to penetrate into the cavities [140, 104, 144]. The shape of the structure top possibly has a pining effect acting as extra resistance to avoid penetration, for instance sharp edge structure [145] or re-entrant like structure [146, 67, 147, 148, 19]. The structure sidewall shape plays a distinct role in liquid penetration [149, 150, 151] as well, which is related with the local breakthrough pressure (the critical wetting pressure when liquid starts to penetrate into the cavity). Hierarchical structures improve the anti-penetration ability [125, 152, 153, 68] by a combination of micro and nano structures compared with both micro structures (where micro structures have low anti-impalement ability) and nano structures (nano structures have high anti-impalement ability but more solid-liquid contact spots where triple-line amount is increased). It has been proposed [154] that the hierarchical structures have nano components and therefore anti-wetting

capillary pressure is high. Additionally, the micro structures impede the development and propagation of pressure waves associated with liquid compression [154]. Finally, hierarchical structures favour mono-stable Cassie state with proper design so that penetrated liquid (into micro structure) could move upward [63, 96] spontaneously.

Conflict in structure design at the same scale

If the liquid penetration is avoided, there is a higher chance to have a bounce-off after droplet impact owing to less energy dissipation. To reduce the energy dissipation at the contact line, lower contact angle hysteresis is desired, which requires a design with less dense and less pinning structures. Here, optimization of the anti-impalement ability and the contact angle hysteresis is conflicting at the same scale. Dense structures or pinning structures top have better anti-impalement ability at the cost of increasing contact angle hysteresis. Energy dissipation during the drop impact process is increased and thus the number of bouncings is weakened. From previous work, the major methods to decouple contact angle hysteresis and anti-impalement ability consist in reducing the structure scale (nano) and increasing the hierarchical level [140, 144]. Conical structures shows high contact angle, low hysteresis and high anti-impalement ability [74, 64], as the conical structures have low solid-liquid contact and no distinct pinning effect on cones top. In Chapter 6, we study the micro pillar sidewall shape effect on droplet impact behavior and report that conical pillar surfaces pose low hysteresis and high anti-impalement ability once designed in a proper way. This paves another way of relaxing the conflict between low hysteresis and anti-impalement capability, in addition to methods like down-scaling of structures or increasing of the hierarchy level [144].

Cassie-Wenzel transition during impact

As mentioned above, in order to get a complete rebound, the surface has to avoid Cassie-Wenzel transition. Previously, the state of energy is compared to show if Cassie-Baxter state or Wenzel state is favored but for a static case only. Here, the impact process is a dynamic process. Thus a force balance model is usually used. Experimental observations have revealed that the wetting transition (transition from bouncing droplet to partial rebound after impact) happens when the impact velocity

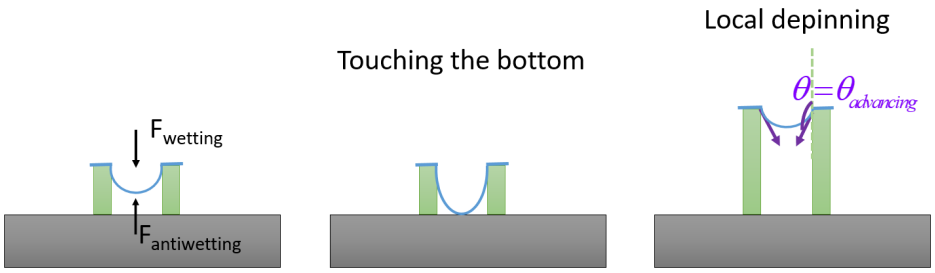

Figure 1-9: Drop impact wetting transition, touching the bottom case and local depinning when local contact angle reaches the advancing angle.

reaches a certain value. It is proposed that transition happens when the liquid either touches the cavity bottom or reaches the local advancing contact angle [110, 143, 155] thus depinning occurs where the liquid could move downward partially or fully to the structure bottom. At either condition, the critical condition is reached when the wetting pressure is equal to the anti-wetting pressure, as demonstrated in Figure 1-9. In previous work, a model equating the dynamic pressure and the Laplace pressure as critical condition [143] is reported for touching the bottom case. The dynamic pressure $P_{dy} = 0.5\rho V^2$ is the wetting pressure, the Laplace pressure $P_L = \frac{2\gamma}{R}$ is the anti-wetting pressure. At the critical condition, the anti-wetting pressure is also called breakthrough pressure. In the case of depinning condition, the liquid might not touch the bottom but still show transition due to the depinning of local triple line when reaching the advancing angle.

The critical condition is then derived when the dynamic pressure is equal to the anti-wetting breakthrough pressure. Here, as we have no detail information about the drop curvature, the local Laplace pressure is unknown. But the anti-wetting ability is from the capillary force, thus the anti-wetting pressure could also be obtained when we know the solid-liquid contact geometry. The anti-wetting pressure P_L is known when we assume the dynamic pressure induced force balances with the capillary force at the triple line, which is further named P_{bk} at the critical depinning condition. Taking the case of cylindrical pillars as an example, equation (1.5) shows the force balance (similar to the classical Jurin's law [156]), written as

$$P_L A + 2\pi r_P \gamma_{LV} \cos(\theta_A) = 0 \tag{1.5}$$

The r_P is the pillar radius and the angle θ_A is the advancing contact angle. The wetting force from the drop impact is the product of the liquid pressure P_L and the acting area A. The capillary force acting around the pillar perimeter $2\pi r_P$ is acting to resist the liquid penetration. The contact area becomes $A = P^2 - \pi r_P^2$, when considering the droplet on a unit cell. Here P is the pillar pitch distance. Using this contact area in equation (1.5), the breakthrough pressure P_{bk} is obtained when $P_L = P_{bk}$, which is written as

$$P_{bk} = \frac{-2\pi r_p \gamma_{LV} \cos\theta_A}{P^2 - \pi r_P^2} \tag{1.6}$$

To enhance the structure resistance to penetration, the anti-wetting pressure can be increased by using a smaller pitch or a larger pillar radius, which results in higher contact angle hysteresis as discussed in the previous section.

Liquid residue after penetration

As discussed previously, the drop impact wetting pressure could overcome the anti-wetting pressure leading to liquid penetration. The breakthrough pressure equation (1.6) shows that the higher pitch and smaller pillar size cases have less anti-penetration ability, which possibly results in more liquid residue. After penetration, liquid residue pins on the surface if spontaneous upward movement is lacking. Several factors affect the residue size. In the literature, it is shown that the liquid residue size is increased when the surface tension is decreased [153] or when the impact velocity is increased [104]. In a lattice Boltzmann simulation work [157], the impact velocity effect is reported as well. Reprinted drop impact images from simulation [157] are shown in Figure 1-10. They [157] proposed that the energy dissipation is strong when liquid is withdrawn from the post thus the number of impaled posts affect the impact outcome, which implies that the actual solid-liquid contact during the impact process is important for liquid residue size. However, the penetrated liquid moves away from the structure [96] for mono-stable Cassie surface as it initiates Wenzel-Cassie

transition spontaneously. But such mono-stable Cassie surfaces still show partial rebound when below a certain temperature owing to condensation effect [96], as shown in Figure 1-11. The lower the temperature the larger the wetted area inside the structure. This work indicates that not only the actual solid-liquid contact matters but also the local solid-liquid adhesion property. Additionally, it is observed that liquid flows both above the structures and also in between the structures [95], which influences the impact outcome. At higher Weber number, they [95] observed that liquid flow inside the grooves dominates, while the flow above the structures dominates at low Weber number. Consequently, the actual solid-liquid contact is complex above and below the structure top, where the flow below the structure top is closely related with the structures sidewall shape. Despite the above mentioned factors influencing the solid-liquid contact size, the role of structures sidewall shape on the liquid residue size has not been studied. The change of sidewall shape can possibly change the solid-liquid contact and thus affect the anti-impalement ability. In addition, the different sidewall shapes have different open lateral space which affects liquid/gas movement in lateral direction. Therefore it is necessary to study the role of sidewall shape. We investigate further the role of sidewall shape on the anti-penetration performance and the liquid residue properties in Chapter 6.

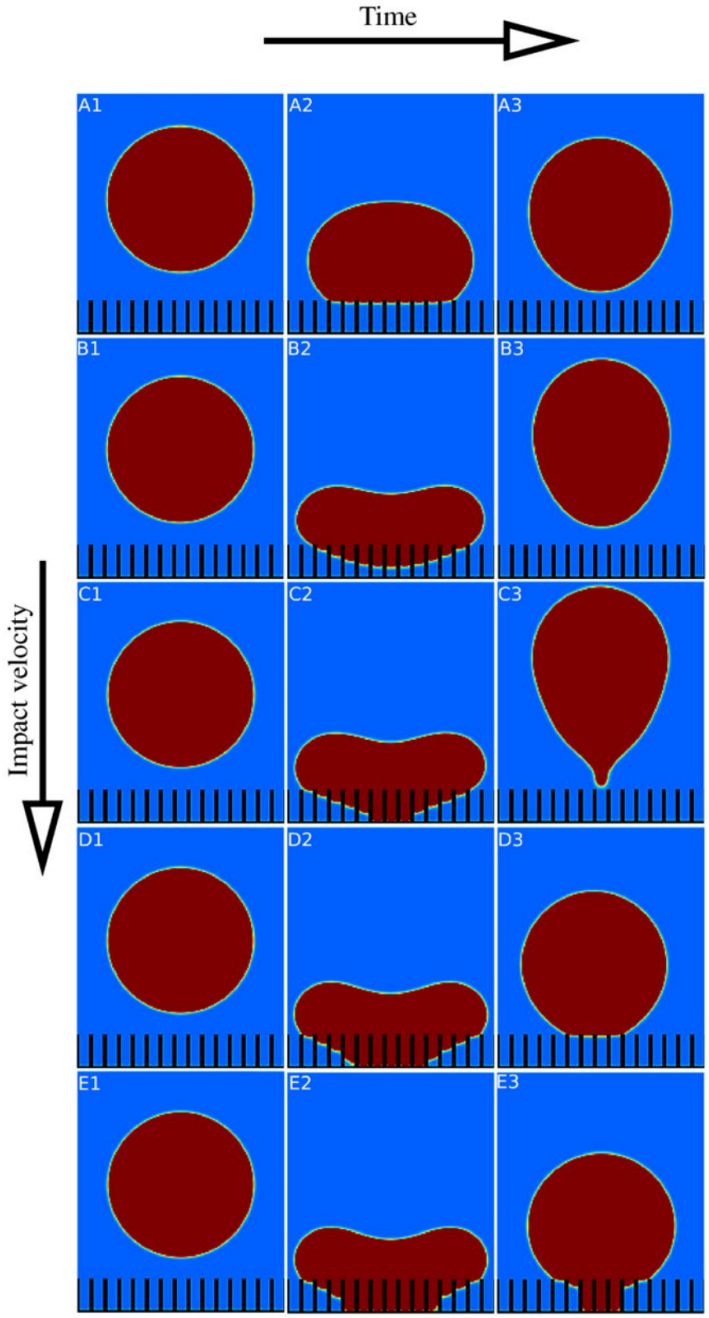

Figure 1-10: Drop impact process from simulations, images reprinted from Hyvaluoma et al.'s work [157]. The liquid partially pins to the surface when the impact velocity is higher.

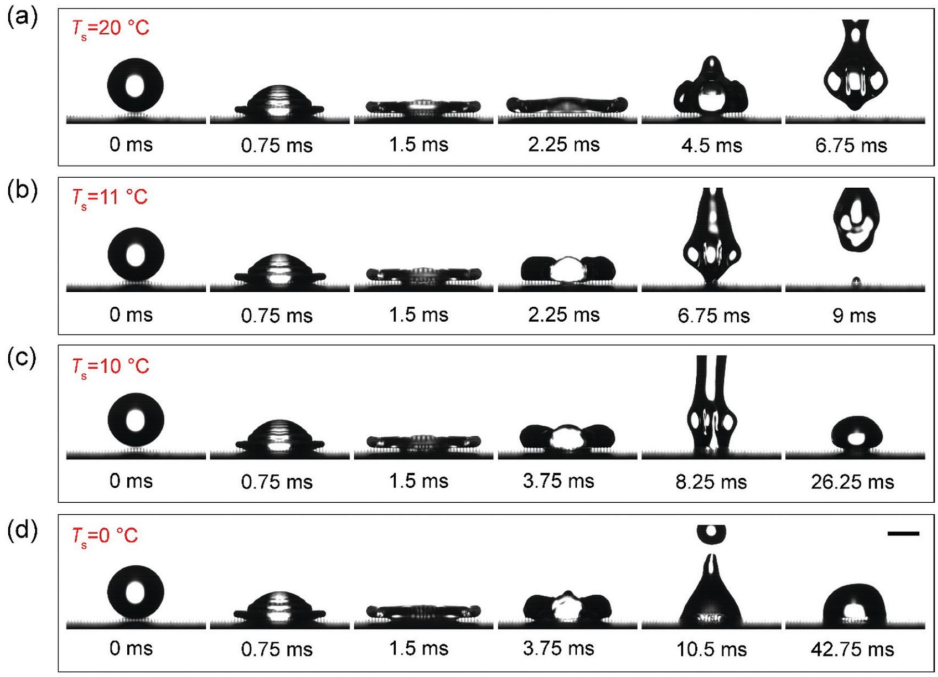

Figure 1-11: Drop impact process for mono-stable Cassie surface, images reprinted from Shi et al.'s work [96].

1.5.5 Droplet bouncing in hydrophilic case

In addition to We number, wettability and roughness also affect the impact behavior. The general outcome can be similar to the one described previously when the surface tension is reduced to the hydrophilic range. Nevertheless, the liquid tends to wet more the surface resulting in gas drainage. Therefore, it is far more difficult to avoid wetting of low surface tension droplets. The most frequently used structure to keep a low surface tension droplet in superhydrophobic state is re-entrant like structures [146, 67, 147, 148, 19]. The re-entrant like structures have a special top to pin the liquid in order to avoid penetration. However, due to the complex fabrication process of re-entrant structures, modified re-entrant surfaces are produced [68, 158, 17, 159, 160, 161, 162]. The modified re-entrant structures are normally not regular like patterned re-entrant structures and the regular cases have complex fabrication process. Therefore, various works adopted simpler ways to produce re-entrant like structures. Other types of nano structures or combination of micro/nano structures have also been reported to show superhydrophobic state for lower surface tension liquids [104, 163, 125, 153, 164]. However, producing a rigid surface capable of repelling lower surface tension liquid impacting at high velocity remains a challenge.

Nano-structures have been used in the literature to achieve better repelling capabilities of a surface by further enhancing the resistance to liquid impalement. In Deng et al.'s work [104], the nano-scale fractal-like silica network surface shows critical Weber number (complete rebound to partial rebound transition) around 4 to 40, for ethanol-water mixtures with γ of 26-72 mN/m. Though the nano-scale structures increase the anti-wetting pressure here, the critical Weber number is not high. They suggest that deeper impalement of liquid inside the nano-network leads to pinning of the impaled liquid at higher We number. In addition to nano structures, several later works adopted micro-nano hierarchical structures to further enhance the repelling property [163, 153, 125], as it is suggested that the micro/nano scale structures can reduce the solid-liquid contact area density but still pose the high anti-wetting pressure. Apart from structure optimization methods, Wong [165] uses surface chemistry

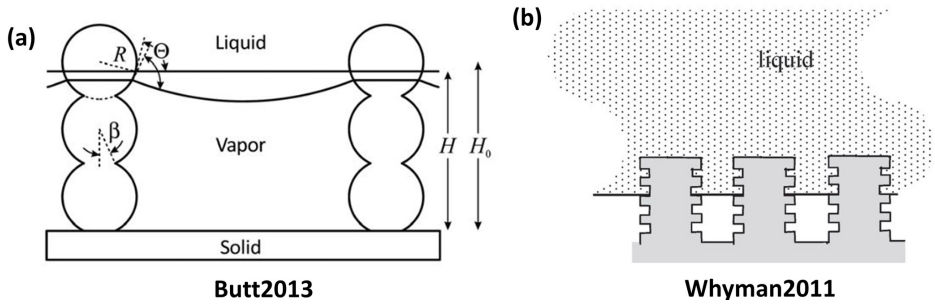

Figure 1-12: Proposed multi-layer sidewall roughness structure in the literature [150, 149].

enhancement to reach super-liquid repellency. This work suggests that liquid penetration resistance is increased by a dense functionalized vertical network of fluoroalkyl on nanoparticles.

The previous mentioned works have revealed that optimization of the structures has to pose both high anti-wetting ability to resist impalement and also low solid-liquid contact area to have as small pining as possible. The reported rigid nano or micro/nano structured surfaces exhibits bouncing of low surface tension drops but stay in Weber number range around 100 or below, which is still some distance to application requirements (applications like inkjet printing [6, 7, 8, 9] and liquid metal printing [10, 11] are involved with higher We number and also lower surface tension liquids). There are several ways to further enhance the anti-wetting ability. Firstly, increased hierarchical level could improve the performance [152]. They suggest that the solid-liquid contact fraction is further reduced by increasing the hierarchical level and also the anti-wetting capillary pressure is increased due to the down-scaling of the structures. Additionally, multi-layer sidewall roughness has been proposed to be a satisfactory pathway [150, 149]. The structure proposed is shown in Figure 1-12. In Pan et al.'s [68] work, they present non-wetting of pentane at Weber number of 250 using multi-re-entrant hierarchical structured woven fabric surfaces. This denotes that an increased level of re-entrant structures is useful for superrepellency of lower surface tension drops at higher Weber number, which might be working for rigid substrates as

well. However, studies using random micro/nano structures are not sufficient to make a conclusion concerning the role of the individual geometry properties, such as pitch and side wall roughness, and how much each of these are responsible for the observed wetting surface properties. In Chapter 5, we contribute to reveal the role of sidewall roughness by studying low surface tension droplet impact on patterned micro conical structures with sidewall roughness. This type of hierarchical structures advance the anti-wetting performance by showing higher critical Weber number, compared with literature works using similar experimental settings.

Chapter 2

Sample fabrication and experiment set-up

In this work, various silicon based pillar structured surfaces are used in the static and dynamic wetting research. The general fabrication process developed in this work for the conical and cylindrical pillars is introduced in this chapter, where Figure 2-1 summarizes the fabrication steps in a schematic way.

2.1 General silicon structured surface fabrication process

Pre-treatment process:

The original 4 inch silicon wafer is at first cleaned by solvents in order to remove dust particle or solvent dissolving dirty things. The silicon wafer is rinsed in solvent, acetone, ethanol, 2-propanol, and de-ionized water in order. Then we dry the wafer by N_2 gas flow. Later, O_2 plasma from a plasma cleaner is further used to clean the wafer.

Coating of photoresist:

In this step, we coat the photoresist onto the clean wafer. In our work, we use negative photoresist Mr-DWL5 following the general process suggested by the resist

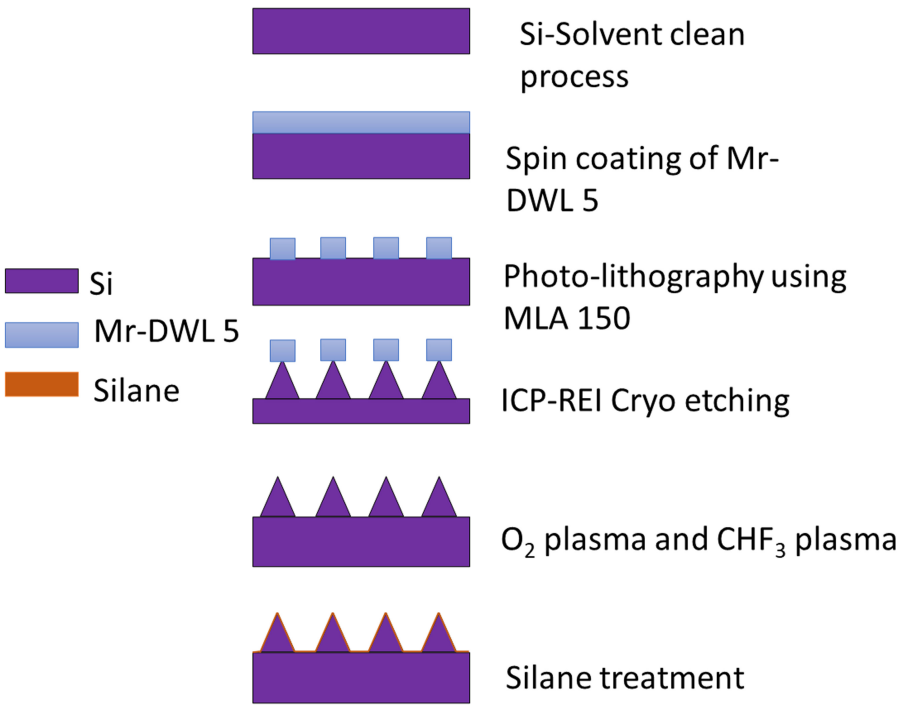

Figure 2-1: Schematic of silicon structured surface fabrication, taking cone production as an example.

provider. The clean wafer is at first baked on a hotplate around 180 $°C$ for 5 minutes. Next we put the wafer on a spin coating device and inject resist in the center of the wafer. We spread the resist uniformly on the wafer by rotating the wafer using 3000 rpm for 30 seconds. When spincoating is finished, the coated wafer has to be pre-baked, with 5 minutes at 50 $°C$, 5 minutes at 90 $°C$ and then 5 minutes at 50 $°C$ again.

Photo-lithography:

The sample from the previous step is then put on a maskless aligner MLA150 (Heidelberg Instruments), in order to expose the pattern we want to use as etching mask. For the mask design, we draw a array of circles with certain pitch and diameter in a GDS file, which can be read by the MLA150 system. We use a laser beam of 405 nm to expose the design resist region at 200-300 mJ/cm^2. After the laser beam exposure, the sample is post-baked at 90 $°C$ for 5 minutes, and another 5 minutes at 50 $°C$ on a hotplate. As we use negative resist, the pattern exposed will be left after putting the sample in a developer, called Mr-dev 600 for around 5 minutes. Isopropanol, de-ionized water, and N_2 gas are used in order to clean and dry the sample. The resist pattern we plan to have is then ready. We use a microscope to check if the developed samples show the desired shape and geometry. This is important step as the resist pattern quality affects the etching quality later.

Plasma etching:

In this step, we will etch the wafer and thus produce the various structures. A lot of work is devoted to the process receipt exploration and optimization for this important and also the most challenging step. Oxford Cryo ICP-RIE dry etching device is utilized to do plasma etching with SF_6/O_2 and CHF_3 as etching gas. In this etching device, we etch into the silicon and thus produce either conical or cylindrical pillar structures. By changing the etching recipe, we achieve control of the pillar height and side wall shape. In theory, the etching gas flow rate, etching temperature, chamber pressure, etching power and etching time all affect the height and shape. From practical etching experience, we found that changing the SF_6/O_2 gas flow is the easiest way to adjust the shape. Changing the etching time is the easiest way

to control the structure height. The chamber pressure influences the shape and the height but the change of pressure frequently reduces stability of the etching power. In several of the etching processes, the etching power is out of tolerance and the device stops the etching process when trying to adjust the pressure. The etching power alters the etch rate distinctly therefore in most cases we use fixed power in a recipe, because a small change of power can have large influence. In short, we normally fix the pressure, the etching power and the temperature and change the gas flow ratio to investigate the recipe for controlling the structures shape. Once the recipe is found, the height can be controlled by the etching time. After finishing the etching, we have the structure we want and then we use O_2 and CHF_3 plasma and to remove the remaining resist or other dirty substances. The conical structures before and after removing the resist are shown in Figure 2-2.

Silane treatment:

Silane (Trichloro(1H,1H,2H,2H-perfluorooctyl)silane, Sigma-Aldrich) treatment (using vacuum silanization tool) is done for 3 hours or overnight to change the intrinsic wetting properties and make the sample superhydrophobic.

2.2 Challenge of fabrication

Plasma etching is flexible to produce different types of pillars. However, the device in hand shows large uncertainty even when we use the same etching recipe, especially when etching at different days.

One of the reasons behind this might be the unstable issue of the device itself. In particular, the chamber pressure and etching power could be unstable sometimes, which will affect the quality of etching. As shown in Figure 2-3, the structure quality is different even using the same etching recipe at the same etching day. Another possible reason is the chamber environment. The device is used by various users and thus there might exist effect from previous user's etching recipe. In addition, the chamber becomes quite dirty after certain time of use. As we are not allowed to change the device itself. Consequently, we try to reduce the latter two problems

by using a chamber cleaning recipe and a pre-conditioning recipe before our actual etching. The chamber cleaning recipe is used to clean the chamber, while the pre-conditioning process is used to bring the device to certain etching condition. However, this is based on practical experience, more research is needed to study how to improve the etching stability.

As mentioned above, repeatability is one of the main challenges. However, for lower aspect ratio pillars the repeatability is satisfying but it is much worse when producing high aspect ratio pillars, especially high aspect ratio conical pillars. Even if we assume the device is in good conditions during etching, we still have difficulty in determining the etching time in an accurate way. As shown in Figure 2-4, if the etching time is not enough, the pillar top will not be sharp when we plan to have cones. With too much etching time, the structures are destroyed to some extent, and black silicon forms randomly. Black silicon is the micro or nano scale random roughness forming after reaching a maximum etching depth. To estimate the required etching time roughly, we need to prepare several wafers with resist mask and use the initial one or two etching results as estimation reference.

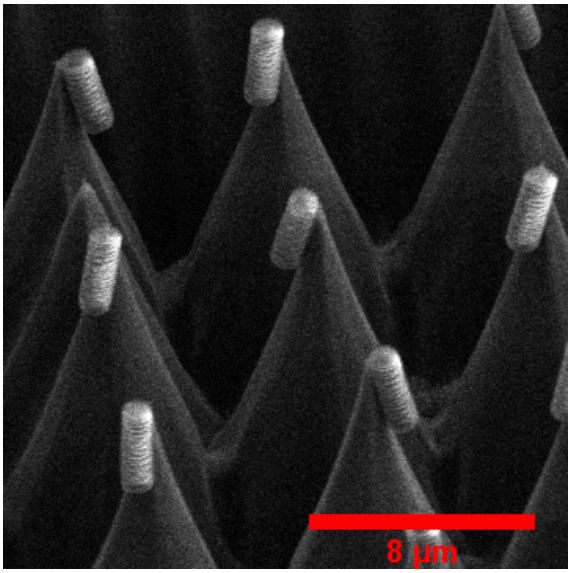

(A)

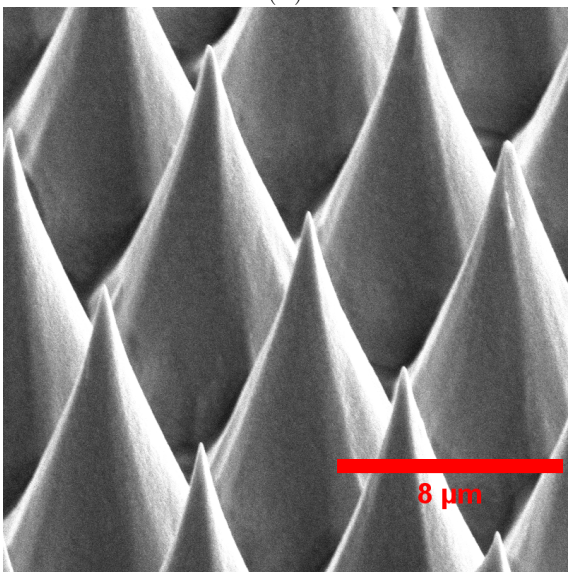

(B)

Figure 2-2: In (A), it shows the SEM image of cone before removing resist. In (B), the same surface is shown after removing the resist. The sample is with pitch 8 μm.

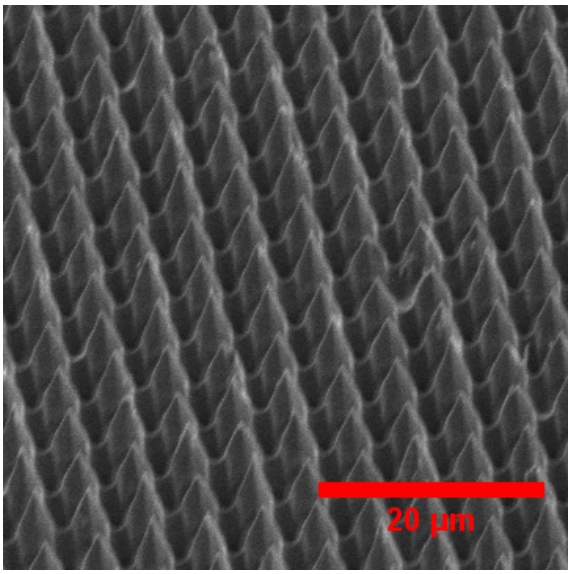

(A)

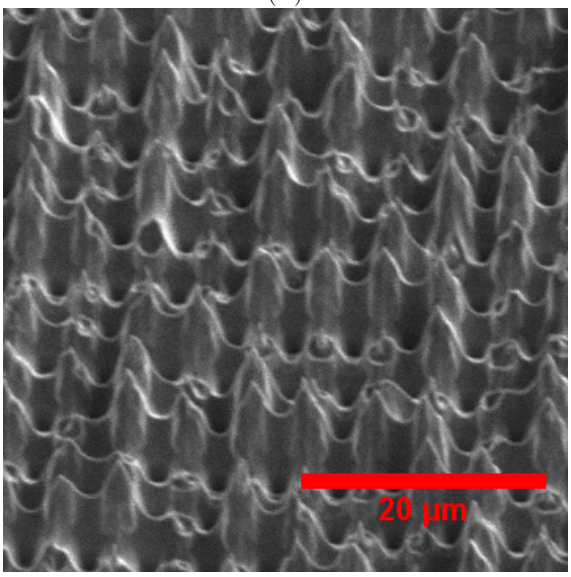

(B)

Figure 2-3: Different quality produced using the same etching receipt and etched at the same day. In (A) , it shows the SEM image of cones in a satisfactory conical shape. In (B), the surface has a lot of heterogeneous and broken parts, where unstable pressure or power is observed during etching.

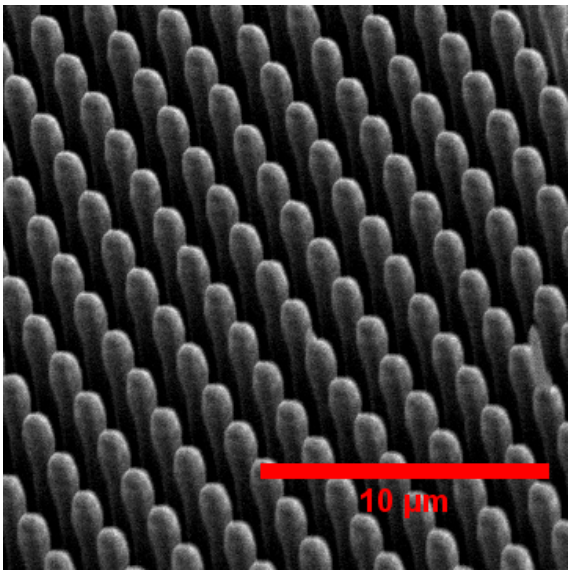

(A)

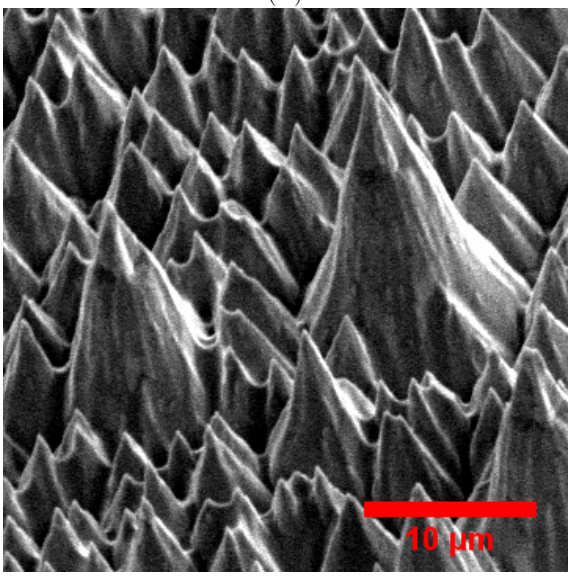

(B)

Figure 2-4: Different etching quality using the same etching recipe but different etching time. In (A) , it shows the SEM image of cones without sharp top, which means the etching is not enough. In (B), etching time is longer but there is a lot black silicon forming, which means the etching is too long.

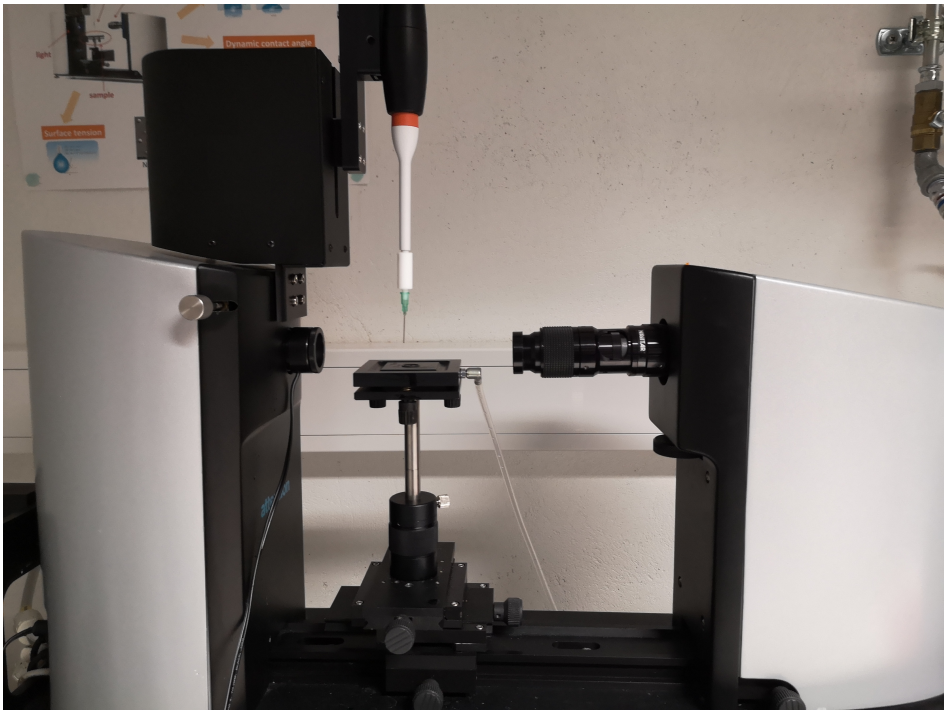

Figure 2-5: OneAttension meter used for contact angle and tilting experiment.

2.3 Experiment set up

2.3.1 Contact angle and tilting experiment

Contact angle for various samples is measured using an optical tensiometer from Biolin Scientific at ambient conditions, as shown in Figure.2-5. The device is at first calibrated using a calibration ball. After calibration, we deposit a droplet with volume 3-11 μl gently on one location of the sample and record the process while the stage is tilted. The whole process is recorded and analyzed using the device software. The static contact angle data can be obtained when the stage is not tilted, while the sliding angle, advancing angle and receding angle can be obtained when the droplet starts to slide. The contact angle hysteresis is the difference between the advancing and receding angles.

Next, we repeat the previous experiment on another sample location. We will repeat at least three times to get an average and dispersion of data. The average value $\overline{x}$ is calculated using $\overline{x} = \frac{\sum_{i=1}^{n} x_i}{n}$. The standard deviation S_x is used to estimate the uncertainty, where $S_x = (\sum_{i=1}^{n} \frac{(x_i - \overline{x})^2}{(n-1)})^{1/2}$.

2.3.2 Drop impact experiment

The droplet impact process is recorded using a high speed imaging system. The experimental setup is shown in Figure 2-6. A syringe is used to dispense a liquid droplet (with volume around 3-10 μl) at a given height above the tested surface. The droplet impact process is recorded using a Photron Fastcam SA3 camera at ambient conditions. In most experiments, 500 frames per second is chosen to have enough window of view to observe the droplet bouncing process. The impact velocity is adjusted by varying the distance of the syringe to the surface.

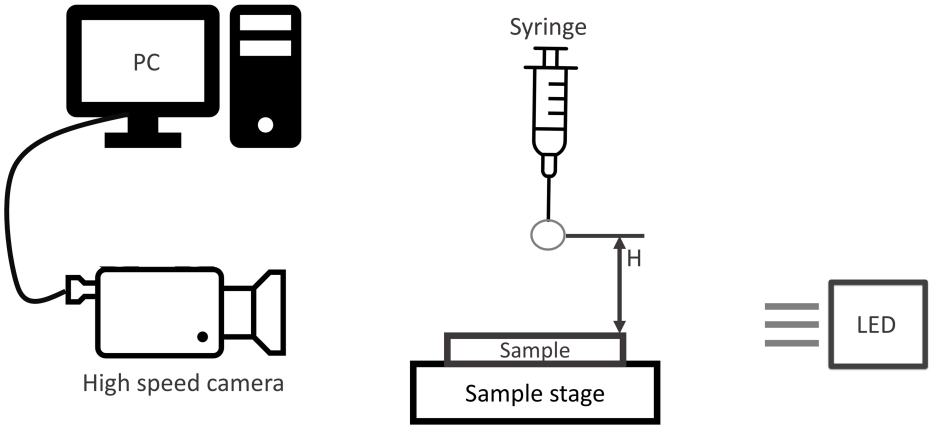

Figure 2-6: Illustration of high-speed imaging set up used for drop impact experiment.

Before starting the impact experiment, we do the calibration by using a calibration ball. Next, we choose an initial needle to surface distance and record the droplet impact for one surface. We repeat at least 3 times at different locations of the surface. After testing one surface, we test different samples at the same distance and also

repeat at least 3 times. We go to another syringe-surface distance and repeat the process again. For critical conditions showing wetting transition, we adjust the needle-to-surface distance in small distance interval, in order to find the condition that starts to show partial rebound for a certain surface. Once the critical distance is found, we repeat at least three times on different locations of the sample to further confirm that the same performance is observed.

From the drop impact experiment, we get the drop radius and drop velocity from the recorded images. We calculate the Weber number ($We = \frac{\rho RV^2}{\gamma}$) based on the measured drop surface tension, calculated drop radius and drop velocity. Therefore, we need to estimate the uncertainty of surface tension, radius, velocity and Weber number for each measurement. The data is from image processing and thus we start with the calibration process. The pixel distance (actual distance per pixel) is calculated by using a known size calibration ball (4 mm in diameter). For each measurement we have 2 pixels uncertainty for the calibration ball diameter. Taking one case as an example, the ball diameter is 220 ± 2 pixels, which results in pixel distance of 18.2 ± 0.2 μm/pixel. When measuring the droplet radius, the error is from the uncertainty of the droplet size in pixels and also error of pixel distance from the calibration. Taking one case of water as an example, we have around 1 pixel error for drop radius thus the drop radius is $R = 62 \pm 1$ pixels. Combining the error from pixel distance as shown above from calibration process using root-sum-square (RSS) method [166], the radius is $R = 1.11 \pm 0.02$ mm. The droplet velocity is calculated by measuring the displacement distance divided by the time difference. By neglecting the error of time, the error of velocity is from distance. For example, at deposition height of 10 mm, the distance traveled in 0.002 s is 44 ± 2 pixels before impact. Combining the pixel distance from calibration with 2 pixels displacement error here using RSS method, the velocity is around $V = 0.40 \pm 0.01$ m/s. The drop surface tension of water is 72 ± 1 mN/m as measured by the pendent drop method. The error of Weber number can be calculated based on error propagation as ($\delta_{We} = \sqrt{\left(\frac{\rho V^2}{\gamma}\right)^2 \delta_R^2 + \left(\frac{2\rho RV}{\gamma}\right)^2 \delta_V^2 + \left(\frac{\rho RV^2}{\gamma^2}\right)^2 \delta_\gamma^2}$, this part of error is also named B as shown below), which results in around 0.1 - 5 error for the range of We numbers

considered in this work (We = 2.4 - 218), the resulting relative error varied between 2% to 5%. When repeating the same type of experiment, there will be random error generated. The standard deviation can be used to quantify this random error but it has to be corrected due to limited sampling size. We use student distribution for this, where $P_{\overline{x}} = \pm t\frac{S_x}{\sqrt{n}}$, here t is value of student distribution which is related with number of sampling and confidence level. With a minimum of 3 repeated experiments, 90% confidence level, t=2.92, thus the random error of the Weber number is in the range of 0.2-17. Combining the error from the previous image processing (B) and the random part (P), the total error ($\delta_{We} = \sqrt{B^2 + P^2}$) of the Weber number is in range of 0.2-19 (We range of 2.4 - 218), and the resulting relative error varied between 3% and 10%.

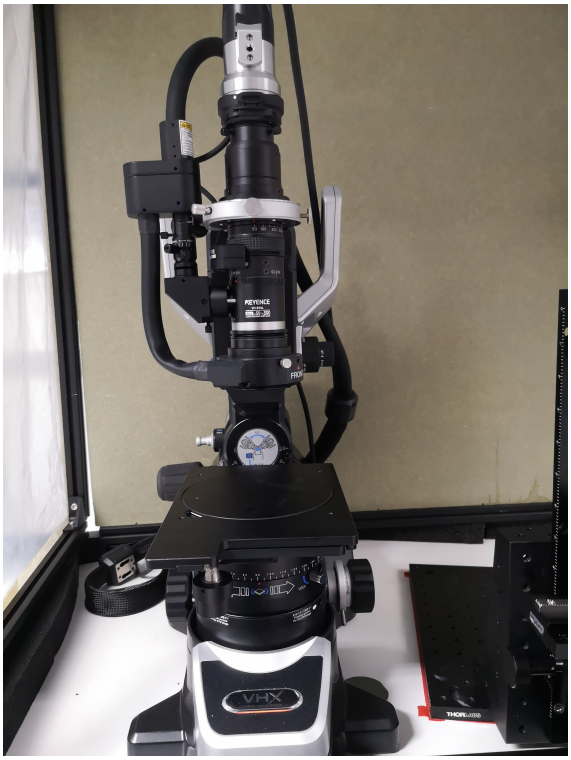

Figure 2-7: Keyence microscope used for drop shape top view imaging.

2.3.3 Top view drop shape imaging experiment

We use a Keyence microscope to record the drop shape from top view, which is shown in Figure 2-7. An ethanol-water mixture or pure ethanol droplet is deposited onto the test surfaces at ambient condition. The droplet diameter size is in the range of 1.7 mm to 1.9 mm. In addition, we also change the distance between the syringe and the surface. The surface on a x-y moving stage is at first placed below the syringe. After depositing a droplet, the sample is moved immediately below Keyence microscope lens and the drop shape is recorded. In this experiment, the main uncertainty is the deposition height. The deposition height is adjusted by hand and quantified using a centimeter ruler. We assumed that the deposition height has around a maximum of 0.5 cm uncertainty.

Chapter 3

Effect of conical micro-pillars on static wetting properties

Brief Summary

In this chapter, we present a study of the effect of conical mciro-pillars on static wetting properties. We produce different conical pillar surfaces and measure the apparent contact angle. It is found that the conical structured surface can show superhydrophobic state for cases with intrinsic contact angle larger than 90°. Besides, we vary the droplet surface tension and measure the contact angle to study the Cassie-Wenzel transition. The results show that the transition from Cassie to Wenzel state is controlled by the conical pillar apex angle. This work contributes to understanding of the effect of conical micro-pillars on static wetting properties and also shows how design of conical structures can be beneficial for reaching super-repellent surfaces.

Applied Physics Letters

Conical micro-structures as a route for achieving super-repellency in surfaces with intrinsic hydrophobic properties

Cite as: Appl. Phys. Lett. **115**, 053703 (2019); https://doi.org/10.1063/1.5096776
Submitted: 19 March 2019 . Accepted: 12 July 2019 . Published Online: 01 August 2019

W. Ding, M. Fernandino, and C. A. Dorao

Applied Physics Letters ARTICLE scitation.org/journal/apl

Conical micro-structures as a route for achieving super-repellency in surfaces with intrinsic hydrophobic properties

Cite as: Appl. Phys. Lett. **115**, 053703 (2019); doi: 10.1063/1.5096776
Submitted: 19 March 2019 · Accepted: 12 July 2019 ·
Published Online: 1 August 2019

W. Ding, M. Fernandino,[a] and C. A. Dorao

AFFILIATIONS

Department of Energy and Process Engineering, Norwegian University of Science and Technology Trondheim 7491, Norway

[a]Electronic mail: maria.fernandino@ntnu.no

ABSTRACT

Hydrophobic surfaces like Lotus leaves show amazing self-cleaning properties with the apparent water contact angle above 150° and contact angle hysteresis below 10°. Thus, at low inclination angles, millimeter drops can roll-off easily. This effect can be a consequence of the air trapped below the drop, which allows the droplet to reach a superhydrophobic Cassie-Baxter state. However, the superhydrophobic state can be accompanied by very different adhesive properties due to the pinning of the droplet to the microstructures, implying that even in a hydrophobic or superhydrophobic state, the droplet might not roll-off easily. A superhydrophobic state with minimum adhesion to the surface has been the pursuit in many applications where a super-repellent state is highly desired. Many microstructures have been shown to be able to reach a superhydrophobic state, but only a few have been shown to be capable of achieving a super-repellent state without the help of more complex hierarchical structures. Here, we show that conical structures provide a template for designing super-repellent surfaces where the wetting characteristics look to be invariant in the microscale range. The conical structures can maintain a super-repellent state for all intrinsic contact angles larger than 90°, and the transition from the Cassie-Baxter to the Wenzel state is controlled by the apex angle of the conical structures. This finding advances the understanding of why conical structures can show a superhydrophobic state, which will be beneficial for the design of super-repellent surfaces with a wider intrinsic contact angle range.

A large number of surfaces[7] have been suggested as possible routes for achieving superhydrophobic surfaces with low adhesive properties and for controlling the motion of the droplets, such as carbon nanotubes,[8] re-entrant structures[9] and multi-re-entrant hierarchical structures,[10] macro-micro-roughness structures,[11] and conical structures.[1,12–14] In particular, conical micro- and nanostructures have been observed to show low adhesive properties, for example, the cicada wings covered by conical protuberances[4] or fabricated surfaces with conelike structures.[1–3,5,6,15] Figure 1 shows some examples of the mentioned conical structures and their wetting properties. Remarkably, although the conical structures have a base diameter in the range of 52 nm to 78 μm, the apparent contact angle and other wetting properties remain similar. These amazing self-repellent wetting properties of the conical structures are the motivation for the work presented here.

We investigate how wetting properties of conical structures are affected by the geometrical properties of the structure. A surface with conical structures can experience two different behaviors that minimize its overall free energy, namely, the Wenzel or the Cassie-Baxter states. In the Wenzel state, the liquid wets the surface completely and the apparent contact angle θ_W^* is given by the modified Young's equation $\cos\theta_W^* = r\cos\theta_e$, with r being the roughness factor defined as the ratio of the actual area of a rough surface to the geometrically projected area and θ_e being the equilibrium contact angle on the flat surface. As r is always greater than unity, the surface roughness enhances the hydrophobicity of a hydrophobic surface. In the Cassie-Baxter state, air intrudes into the hydrophobic solid-liquid interface, and thus, the droplet is lying over an interface composed of part solid and part air. The apparent contact angle θ_A^* is given by $\cos\theta_A^* = f_1\cos\theta_1 + f_2\cos\theta_2$[16] where f_1 is defined as the total area of the solid under the drop per unit projected area under the drop, θ_1 is the equilibrium contact angle on a smooth surface of material 1, and f_2 is defined as f_1 but for air and $\theta_2 = 180°$.[17]

For understanding the wetting properties of the conical structures and their favorability to each state, the stability criterion can be written as $\cos\theta_C = -f_2/(r - f_1)$,[17,18] which is the angle obtained when equating the Wenzel and Cassie-Baxter equations. This implies that if

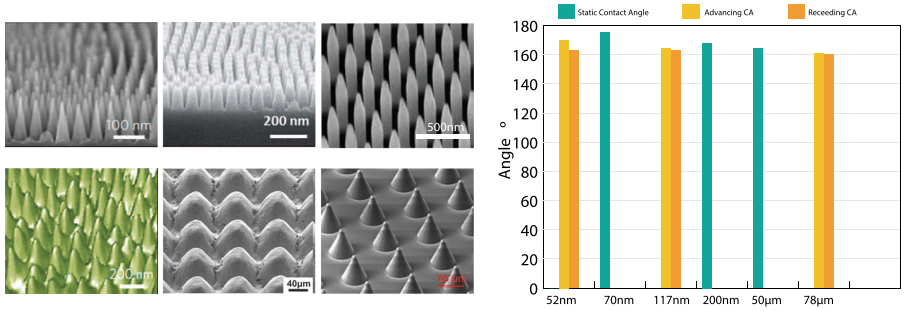

FIG. 1. Example of conical-like structures from nature and artificially fabricated structures, Permissions (from first row, left to right order): reproduced with permission from Mouterde *et al.*, Nat. Mater. **16**, 658–663 (2017). Copyright 2017 Springer Nature. Reproduced with permission from Telecka *et al.*, RSC Adv. **8**, 4204–4213 (2018). Copyright 2018 The Royal Society of Chemistry. Reproduced with permission from Martines *et al.*, Nano Lett. **5**(10), 2097–2103 (2005). Copyright 2005 American Chemical Society. Reproduced with permission from Wisdom *et al.*, Proc. Natl. Acad. Sci. **110**(20), 7992–7997 (2013). Copyright 2013 Proceedings of the national Academy of Sciences of the United States of America. Reproduced with permission from Sharma *et al.*, ACS Appl. Mater. Interfaces **10**(34), 29127–29135 (2018). Copyright 2018 American Chemical Society. Reproduced with permission from Park *et al.*, Adv. Mater. Interfaces **5**(5), 1701039 (2018). Copyright 2018 John Wiley and Sons. Contact angle data are remarkably independent of the scale of the structure.

$\theta_C < \theta_e$, the droplet will favor the Cassie-Baxter state. The maximum theoretical contact angle on a flat surface is about 120° which can be achieved by lowering the surface energy and corresponds to the lowest surface energy value yet recorded of 6 mJ m^{-2} for a surface with a regularly aligned closest-hexagonal-packed -CF3 group.[19] Figure 2(a) shows the influence of the half apex angle of the conical structures β and the penetration of the liquid into the structures ϕ in the wetting state. This implies that conical structures with a half apex angle larger than 20° might favor the Wenzel state. The apparent contact angle θ^* corresponding to the Cassie-Baxter model can be determined assuming the given penetration of the liquid into the structures as shown in Fig. 2(b). This shows that cones with a high aspect ratio favor a superhydrophobic state as $\theta_e \to 90°$. But this estimation depends on the penetration of the liquid into the structures which needs to be determined. Considering a force balance between the surface force and the liquid pressure, it is possible to determine the liquid penetration as a function of θ_e–β and the diameter base of the cones or pitch for millimeter size drops. As shown in Figs. 2(c) and 2(d), the conical structures are capable of supporting a drop even for relatively high pitches, corresponding to microsized cones. However, for nanosized cones, the penetration of the liquid is minimized, and thus, the adhesion force can be reduced to its minimum. This property can be hindered by the transition from the Cassie-Baxter to the Wenzel state, which can occur either spontaneously or induced by external stimuli. Figure 3 shows in

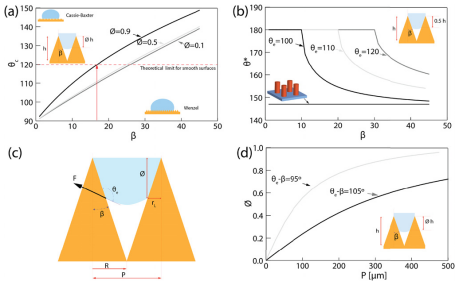

FIG. 2. Wetting characteristics of conical structures. (a) Illustration of the influence of the half apex angle of the cones on the stability criterion limiting the Cassie-Baxter and Wenzel states. (b) Effect of the half apex angle of the cones and the equilibrium contact angle on the apparent contact angle. This result suggests that surfaces with a small half apex angle of the cones will show superhydrophobic behavior. (c) and (d) show the effect of the pitch on the liquid penetration on the structure.

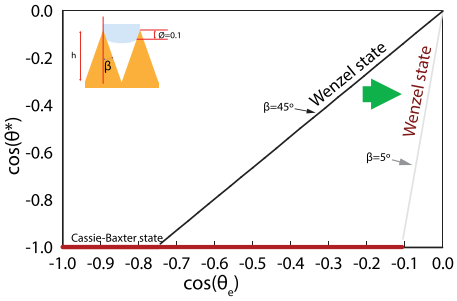

FIG. 3. Effect of the half apex angle on the transition from the Cassie-Baxter to Wenzel states in the Kao diagram. Sharp conical structures can suppress the Wenzel state in the 3rd quadrant of the Kao diagram.

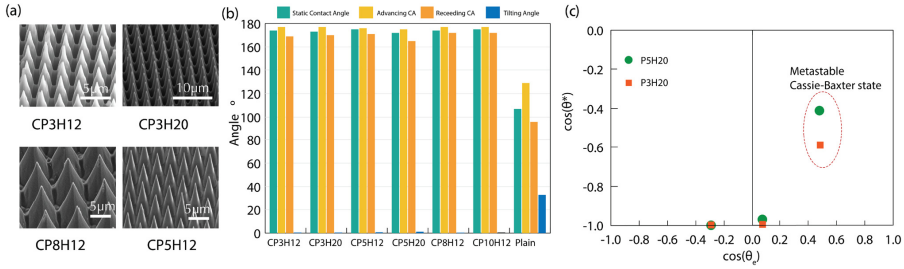

FIG. 4. (a) Examples of scanning electron microscopy images of the fabricated conical structures, where P is the pitch and H is the height of the structures, both in micrometers. (b) Contact angle data of the fabricated conical structures showing a remarkably superhydrophobic state for the geometries fabricated. (c) Kao diagram for two conical structures confirming the suppression of the Cassie-Baxter to Wenzel states.

the Kao diagram[18,20,21] the effect of the apex angle on the apparent contact angle under equilibrium conditions. As the apex angle goes to zero, the transition from the Cassie-Baxter to Wenzel states moves to lower equilibrium contact angles, suppressing the Wenzel state in the negative quadrant corresponding to $\cos\theta_e < 0$. Therefore, conical structures can allow a superhydrophobic state and low adhesion for liquid with $\theta_e > 90°$ for low half apex angles. The transition from the Cassie-Baxter to Wenzel states induced by external stimuli has been observed under evaporation,[22,23] vibration,[24] bouncing of droplet,[25,26] and pressing.[27] In spite of the substantial research in this area, the quantification of the capability of the surface for controlling the occurrence of the wetting transition remains challenging and the analysis needs to take into account the time scale of the transition which can be characterized by a rapid adiabatic or slow nonadiabatic one.[28] Due to the level of complexity of the problem, in this case, we assume the situation of the wetting transition triggered by the impact of a falling droplet. The transition can be assumed to be triggered when the dynamic pressure $p_d = 1/2\rho V^2$ overcomes the Laplace pressure $p_L = 2\ \gamma/R$, with R being the radius of curvature of the liquid when it touches the bottom of the surface.[26] Alternatively, it is possible to consider that at the transition condition, the liquid interface should sustain its advancing contact angle. Then, the pressure force supported by one conical structure $f = 2\pi r_L\gamma\ \cos(\theta_a - \beta)$ should be counterbalance by the force exerted by the dynamic pressure $f_d = 1/2\rho V^2 P^2$. Therefore, the transition will occur for impact velocities higher than $V_c > [2\pi r_L\gamma\ \cos(\theta_a - \beta)/(1/2\rho\, P^2)]^{1/2}$, where $r_L = P\ \phi/2$. Hence, the critical velocity increases as the pitch parameter P decreases as $V_c \propto P^{-1/2}$, and the critical velocity reaches an optimum as the half apex angle of the cones tends to zero. The previous results suggest that low pitch conical structures with a small half apex angle provide a route for achieving super-repellency on surfaces with intrinsic hydrophobic properties.

Inspired by the discussed wetting properties of conical structures, a series of surfaces with microconical structures have been fabricated. The cones were designed to have spacing or pitch, P, equal to the diameter of the base of the cones. The fabricated cones have pitches of 3, 5, 8 and 10 μm and heights of 12 and 20 μm which result in half apex angles from 4° to 23°. The surfaces are rendered hydrophobic by vapor deposition of 1H,1H,2H,2H-Perfluorooctyl-trichlorosilane. On a flat silicon, this treatment provides an equilibrium contact angle of 107° ± 3°, a contact angle hysteresis of 32° ± 2°, and a tilting angle of 33° ± 2°.

Figure 4(a) shows some examples of the conical structures using a Scanning Electron Microscope FEI SEM APREO. As an abbreviation rule, C refers to the cone, P is the pitch, and H is the height so that CP3H12 is a surface with cones with a pitch of 3 μm and a height of 12 μm. All the surfaces show an apparent contact angle ranging from 172° to 175° for water droplets of 5.4 to 7 μl. Furthermore, all the surfaces show a low contact angle hysteresis of 5° to 8° and a tilting angle smaller than 1°, as depicted in Fig. 4(b). The values of the contact angle are higher than the ones reported in the literature. Figure 1 and this can be due to the accuracy of triple-line detection.

The contact angle hysteresis of the fabricated microcones is quite similar to the one corresponding to nanocones,[2,3] showing that the geometrical property of the cones is valid in the micro and nanosize range. The sliding test for some of the surfaces is shown in Fig. 5 for the plain surface and two surfaces with microcones. The low sliding angle suggests that the droplet is in a Cassie state. For all the tested surfaces with microcones, no effect on the sliding angle to the degree of accuracy of the instrument has been observed.

In order to investigate the effect of the equilibrium contact angle on the apparent contact angle, as presented in Fig. 3, in Fig. 4(b), the

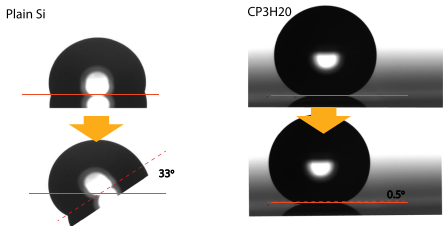

FIG. 5. The sequence illustrates the substantial reduction in the adhesion force on the surface with conical structures CP3H20 compared to the plain Si surface.

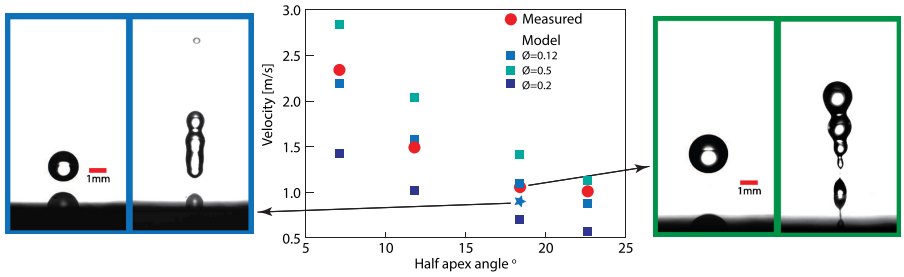

FIG. 6. The measured critical velocity for conical structures with a height of 12 μm and different half apex angles is presented and compared with the model of the critical velocity for different penetration parameters ϕ.

apparent contact angle was varied by mixing water and isopropanol at different percentages which changes the surface tension of the liquid. The equilibrium contact angle was evaluated on a plain surface with equivalent treatment compared to the conical structures. The conical structure CP3H20 shows a superhydrophobic state even at an equilibrium contact angle of 86°. It is also possible to observe that the apparent contact angle in the metastable Cassie-Baxter state has also been enhanced by reducing the half apex angle in the structures. Finally, in Fig. 6, the robustness of the surface for avoiding the transition from the Cassie-Baxter to Wenzel states under impacting droplets is presented. In this case, droplets of 2.2 ± 0.1 mm impact a conical surface CP3H12 at different velocities. The velocity, at which a transition from the Cassie-Baxter to Wenzel states is observed, is defined as the critical velocity. The model for different penetration parameters ϕ is included in the plot showing a comparable trend with the experiments. A maximum critical velocity of 2.3 ± 0.2 m/s has been achieved for the sample corresponding to conical surface CP3H12. It can be noticed that experiments performed with pillar structures have shown lower critical velocities of about 1.1m/s for pillar structures of 5 μm in diameter, 7 μm in pitch, and 10 μm in height for droplets of 1 mm in diameter.[26] For the case of droplets of 1 mm in diameter impacting pillar structures of diameter 22 μm, pitch 50 μm, and height 9 μm, critical velocities of about 0.8 m/s have been observed.[25] A possible alternative for increasing the critical velocity is by increasing the number of tiers of roughness of the surface.[25]

Our results show that conical structures are capable of achieving super-hydrophobic conditions for microsized features. In particular, the apex angle of cones and the intrinsic contact angle are the dominant parameters when designing the surfaces. Reducing the pitch between the cones contributes to enhancing the robustness of the surface, while reducing the apex angle of the cones allows us to suppress the Wenzel state for hydrophobic materials.

See the supplementary material for the details of the experiments and fabrication process.

The Research Council of Norway is acknowledged for the support to the Norwegian Micro- and Nano-Fabrication Facility, NorFab (No. 245963/F50).

REFERENCES

[1]T. Mouterde, G. Lehoucq, S. Xavier, A. Checco, C. T. Black, A. Rahman, T. Midavaine, C. Clanet, and D. Quéré, "Antifogging abilities of model nanotextures," Nat. Mater. **16**, 658–663 (2017).
[2]A. Telecka, T. Li, S. Ndoni, and R. Taboryski, "Nanotextured Si surfaces derived from block-copolymer self-assembly with superhydrophobic, superhydrophilic, or superamphiphobic properties," RSC Adv. **8**, 4204–4213 (2018).
[3]E. Martines, K. Seunarine, H. Morgan, N. Gadegaard, C. D. Wilkinson, and M. O. Riehle, "Superhydrophobicity and superhydrophilicity of regular nanopatterns," Nano Lett. **5**, 2097–2103 (2005).
[4]K. M. Wisdom, J. A. Watson, X. Qu, F. Liu, G. S. Watson, and C.-H. Chen, "Self-cleaning of superhydrophobic surfaces by self-propelled jumping condensate," Proc. Natl. Acad. Sci. **110**, 7992–7997 (2013); e-print arXiv:1406.7436.
[5]C. S. Sharma, C. Stamatopoulos, R. Suter, P. R. V. Rohr, and D. Poulikakos, "Rationally 3D-textured copper surfaces for Laplace pressure imbalance-induced enhancement in dropwise condensation," ACS Appl. Mater. Interfaces **10**, 29127–29135 (2018).
[6]I. Park, M. Fernandino, and C. Dorao, "Wetting state transitions over hierarchical conical microstructures," Adv. Mater. Interfaces **5**, 1701039 (2018).
[7]M. Liu, S. Wang, and L. Jiang, "Nature-inspired superwettability systems," Nat. Rev. Mater. **2**, 17036 (2017).
[8]P. Joseph, C. Cottin-Bizonne, J. M. Benoit, C. Ybert, C. Journet, P. Tabeling, and L. Bocquet, "Slippage of water past superhydrophobic carbon nanotube forests in microchannels," Phys. Rev. Lett. **97**, 1–4 (2006); e-print arXiv:0609043 [cond-mat].
[9]A. Tuteja, W. Choi, J. M. Mabry, G. H. McKinley, and R. E. Cohen, "Robust omniphobic surfaces," Proc. Natl. Acad. Sci. **105**, 18200–18205 (2008); e-print arXiv:0811.2183v2.
[10]S. Pan, R. Guo, M. Björnmalm, J. J. Richardson, L. Li, C. Peng, N. Bertleff-Zieschang, W. Xu, J. Jiang, and F. Caruso, "Coatings super-repellent to ultralow surface tension liquids," Nat. Mater. **17**, 1040–1047 (2018).
[11]J. C. Bird, R. Dhiman, H. M. Kwon, and K. K. Varanasi, "Reducing the contact time of a bouncing drop," Nature **503**, 385–388 (2013); e-print arXiv:1011.1669v3.
[12]B. D'Urso, J. T. Simpson, and M. Kalyanaraman, "Emergence of superhydrophobic behavior on vertically aligned nanocone arrays," Appl. Phys. Lett. **90**, 044102 (2007).
[13]K. Li, J. Ju, Z. Xue, J. Ma, L. Feng, S. Gao, and L. Jiang, "Structured cone arrays for continuous and effective collection of micron-sized oil droplets from water," Nat. Commun. **4**, 2276 (2013).
[14]A. Checco, B. M. Ocko, A. Rahman, C. T. Black, M. Tasinkevych, A. Giacomello, and S. Dietrich, "Collapse and reversibility of the superhydrophobic state on nanotextured surfaces," Phys. Rev. Lett. **112**, 1–5 (2014).
[15]E. Hosono, S. Fujihara, I. Honma, and H. Zhou, "Superhydrophobic perpendicular nanopin film by the bottom-up process," J. Am. Chem. Soc. **127**(39), 13458–13459 (2005).

[16]D. Quéré, "Wetting and roughness," Annu. Rev. Mater. Res. **38**, 71–99 (2008).
[17]A. J. Milne and A. Amirfazli, "The Cassie equation: How it is meant to be used," Adv. Colloid Interface Sci. **170**, 48–55 (2012).
[18]J. Bico, U. Thiele, and D. Quéré, "Wetting of textured surfaces," Colloids Surf. A **206**, 41–46 (2002).
[19]Y. T. Cheng and D. E. Rodak, "Is the lotus leaf superhydrophobic?," Appl. Phys. Lett. **86**, 144101 (2005).
[20]J. Zeegers, D. V. D. Ende, and F. Mugele, "Trapping of drops by wetting defects," *Nature Communications* **5**, 3559 (2014).
[21]J. Kujawa and W. Kujawski, "Functionalization of ceramic metal oxide powders and ceramic membranes by perfluoroalkylsilanes and alkylsilanes possessing different reactive groups: Physicochemical and tribological properties," ACS Appl. Mater. Interfaces **8**(11), 7509–7521 (2016).
[22]G. McHale, S. Aqil, N. J. Shirtcliffe, M. I. Newton, and H. Y. Erbil, "Analysis of droplet evaporation on a superhydrophobic surface," Langmuir **21**, 11053–11060 (2005).
[23]S. Moulinet and D. Bartolo, "Life and death of a fakir droplet: Impalement transitions on superhydrophobic surfaces," Eur. Phys. J. E **24**, 251–260 (2007).
[24]E. Bormashenko, R. Pogreb, G. Whyman, Y. Bormashenko, and M. Erlich, "Vibration-induced Cassie-Wenzel wetting transition on rough surfaces," Appl. Phys. Lett. **90**, 2005–2007 (2007).
[25]D. Bartolo, F. Bouamrirene, É. Verneuil, A. Buguin, P. Silberzan, and S. Moulinet, "Bouncing or sticky droplets: Impalement transitions on superhydrophobic micropatterned surfaces," Europhys. Lett. **74**, 299–305 (2006).
[26]Y. C. Jung and B. Bhushan, "Dynamic effects of bouncing water droplets on superhydrophobic surfaces," Langmuir **24**, 6262–6269 (2008).
[27]A. Lafuma and D. Quéré, "Superhydrophobic states," Nat. Mater. **2**, 457–460 (2003).
[28]E. Bormashenko, "Progress in understanding wetting transitions on rough surfaces," Adv. Colloid Interface Sci. **222**, 92–103 (2015).

Conical micro-structures as a route for achieving super-repellency in surfaces with intrinsic hydrophobic properties
Supplemental information

W. Ding,[1] M. Fernandino,[1, a)] and C.A. Dorao[1]
Department of Energy and Process Engineering. Norwegian University of Science and Technology Trondheim, 7491, Norway.

(Dated: 26 June 2019)

I. SAMPLE FABRICATION AND CHARACTERISATION

A. Sample fabrication

First, the silicon wafer was rinsed in solvent, acetone, ethanol, isopropanol and deionized water. The wafer was then dried with N_2. The samples were then coated with negative photoresist Mr-dwl-5 at 3000 rpm for 30 seconds and the samples were prebaked. Next, a given pattern was directly exposed on the photoresist by using a mask aligner MLA150 (Heidelberg Instruments) with a light source at 405nm. The silicon wafers were patterned with a square arrangement of circles, each circle with diameter of 1 micro meter and pitch of 3 μm, 5μm, 8μm and 10 μm in each sample respectively. The samples were developed using developer Mr dev 600. An Oxford Cryo ICP-RIE dry etching device was utilized to do plasma etching with SF_6/O_2 and CHF_3. A silane (Trichloro(1H,1H,2H,2H-perfluorooctyl)silane,Sigma-Aldrich) treatment (using vacuum silination tool) was performed for 3 hours to make the samples superhydrophobic. A schematic representation of the production process is shown in FIG 1.

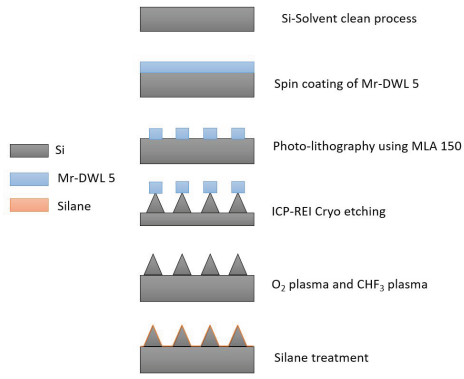

Fig. S. 1: Schematic representation of fabrication of conical pillars.

Six samples with conical structures were produced from three different etching conditions. As shown in FIG 2, the conical structures produced here are closely packed, meaning that the base diameter is nearly the same as the pitch (center to center distance, design value for the four region is 3, 5, 8, 10 μm). Sample B is not so densely packed but the base diameter is close to the pitch. It is worth mentioning that the 3 μm pitch samples not only have conical pillars but they also have a truncated cone hole in between the pillars. In FIG 2, samples A, C and F are all produced using the same recipe (SF_6/O_2-85/16 sccm, pressure 50 mTorr, 10 minutes, O_2 plasma 10 min, then CHF_3 5 minutes). For sample B a different recipe was used (SF_6/O_2-85/16 sccm, pressure 20 mTorr, 10 minutes, O_2 plasma 10 min, and CHF_3 5 minutes). The parameters for sample D and E are the same (SF_6/O_2-85/16 sccm, pressure 30 mTorr, 14 minutes, O_2 plasma 10 min, and CHF_3 5 minutes). For all etching processes and recipes, the temperature was -50°C. All samples were subject to a process of O_2 plasma cleaning (40 O_2 sccm, pressure 20 mTorr, 15 minutes) to remove any remaining photoresist. The smooth hydrophobic silicon surface was treated with a CHF_3 plasma for 5 min and silane for 3 hours, so that all samples had the same surface conditions.

a) Electronic mail: maria.fernandino@ntnu.no.

B. SEM characterisation

SEM of conical pillars In FIG2, the scanning electron microscope (SEM) images are presented. A FEI SEM APREO was used to characterize the conical pillar surface. Four of the samples have height around 12 μm (namely samples A, B, C and F) and two samples have a height of 20 μm (samples D and E).

II. CHARACTERIZATION OF SURFACES WETTING PROPERTIES

A. Wetting property with pure water

Contact angle was measured at ambient conditions using an optical tensiometer from Biolin Scientific. A droplet of deionized water with diameter 5.4-7 μl was deposited on one location of the sample. The sample was tilted continuously while the whole process was recorded by a camera, until the droplet would start sliding. The same procedure was then repeated on another point of the sample. It is worth mentioning that the droplet size used for the smooth hydrophobic silicon surface was much larger, namely 15-17 μl, since hysteresis is larger for this sample and the droplet would not slide below a certain size. All the process was repeated at least three times and average values over all the runs are reported. The wetting data for pure water is summarized in TABLE I, in which θ_A is the advancing contact angle, θ_R is the receding contact angle, α_T is the tilting angle when droplet slides and θ_A^* is the static contact angle.

Table S. I: Contact angle on conical structures with pure water

Sample	θ_A	θ_R	θ_A-θ_R	α_T	θ_A^*
CP3H12	177 ± 1°	169 ± 3°	8 ± 3°	0.5 ± 0.4°	174 ± 3°
CP5H12	177 ± 3°	170 ± 1°	7 ± 2°	0.5 ± 0.1°	173 ± 1°
CP8H12	176 ± 2°	171 ± 1°	5 ± 3°	0.8 ± 0.1°	175 ± 2°
CP10H12	175 ± 2°	165 ± 3°	9 ± 5°	1.2 ± 0.7°	172 ± 1°
CP3H20	177 ± 2°	172 ± 3°	5 ± 3°	0.4 ± 0.1°	174 ± 1°
CP5H20	177 ± 1°	172 ± 1°	5 ± 1°	0.5 ± 0.1°	175 ± 1°
Si smooth	129 ± 4°	96 ± 2°	32 ± 3°	33 ± 2°	107 ± 3°

B. Wetting property with isopropanol-water mixture

In order to change the wetting angle without modifying the surface, the static contact angle was further tested using mixture of isopropanol (2-Propanol for analysis EMSURE ® ACS, ISO, Reag. Ph Eur) and deionized water.

Test process: isopropanol and water were mixed in a certain ratio and the liquid mixture surface tension was measuring using an optical tensiometer from Biolin Scientific with the pendent drop method. The mixture was the used to measure the static contact angle on both a flat silicon surface and the surfaces with conical structures.

Two types of mixtures were used here:

Mixture 1: 5 ml isopropanol and 45 ml water with surface tension 46 ± 4 mN/m and contact angle on smooth hydrophobic surface of 86± 6°.

Mixture 2: 10 ml isopropanol and 30 ml water with surface tension 35 ± 4 mN/m and contact angle on smooth hydrophobic surface of 61±3°. The results for the static contact angle on conical structures are listed in TABLE II.

Results for mixture 1 show that conical pillars can result in a superhydrophobic state even for equilibrium contact angle of $\theta_e = 86 \pm 6°$ on a smooth surface with the same intrinsic wetting properties. This shows that the Wenzel state is suppressed by the conical structures. The static contact angle of mixture 2 is lower, but it is still in hydrophobic condition, which is a meta-stable state.

Table S. II: Contact angle on conical structures with isopropanol-water mixtures

Sample	θ_A^* of mixture 1	θ_A^* of mixture 2
CP3H12	171 ± 1°	113 ± 6°
CP5H12	171 ± 2°	111 ± 5°
CP8H12	167 ± 4°	115 ± 8°
CP10H12	167 ± 3°	114 ± 4°
CP3H20	174 ± 2°	126 ± 3°
CP5H20	166 ± 2°	114 ± 8°
Si smooth θ_e	86 ± 6°	61 ± 3°

C. Contact angle and droplet volume

The contact angle as a function of droplet volume is shown in FIG.3. The results here indicate that the contact angle is quite stable in the measured volume range for the cone CP3H12.

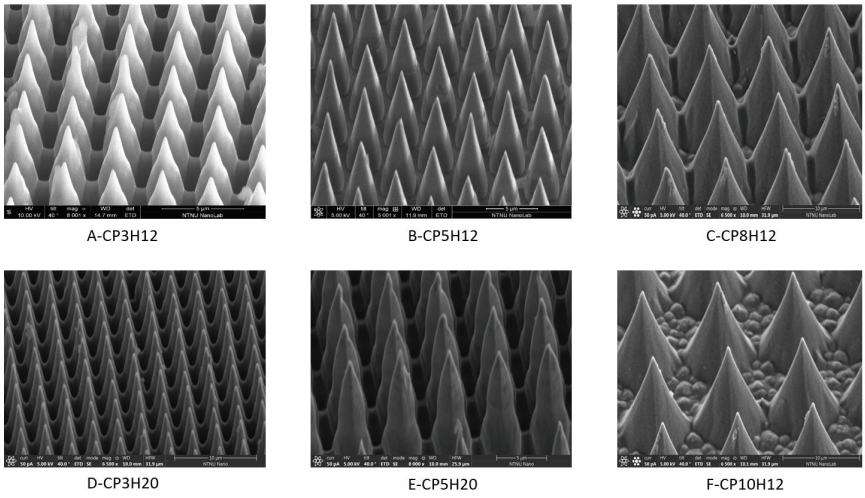

Fig. S. 2: SEM images of conical pillars.

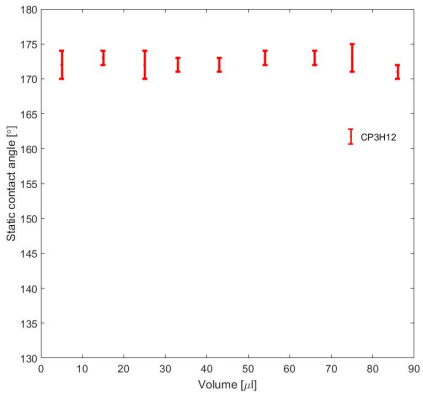

Fig. S. 3: Contact angle as a function of droplet volume.

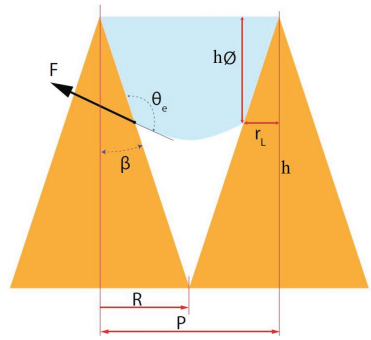

Fig. S. 4: Schematic of cone geometry.

III. SUMMARY OF WETTING MODEL USED

Cassie-Baxter model[1]:

$$\cos\theta_A^* = f_1 \cos\theta_e - f_2 \tag{S1}$$

The angle θ_A^* is the apparent contact angle, f_1 is the actual solid-liquid contact fraction, f_2 is the solid-air fraction; The θ_e is the equilibrium contact angle on flat surface;

The stability criterion is got by equating Cassie-Baxter equation and Wenzel equation[2].

$$\cos\theta_C = -f_2/(r - f_1) \tag{S2}$$

The angle θ_C is the critical contact angle, r is roughness factor, which means the product of total surface area

dividing the projected surface area. Based on conical structure geometry, as shown in FIG.4, these data can be calculated assuming certain penetration depth fraction ϕ. The β is half apex angle.

$$f_2 = \frac{P^2 - r_L^2\pi}{P^2} \tag{S3}$$

$$f_1 = \frac{\pi r_L^2}{P^2 \sin(\beta)} \tag{S4}$$

$$r = 1 - \frac{\pi R^2}{P^2} + \frac{\pi R^2}{P^2 \sin(\beta)} \tag{S5}$$

$$r_L = R^* \phi \tag{S6}$$

Force balance: the capillary force is balanced with the liquid pressure force.This force balance equation can relate the penetration fraction ϕ with the angle $(\theta_e - \beta)$.

$$\frac{2\gamma_{LV} A}{R_e} - 2\pi r_L \gamma_{LV} \cos(\theta_e - \beta) = 0 \tag{S7}$$

In the above equation, the γ_{LV} is liquid-vapor surface tension, r_L is the wetted radius, R_e is the interface curvature, as this is unknown but the curvature assumed be similar in all surfaces as the droplet is deposited on the surface gently, thus in the calculation, constant interface curvature is used; The liquid pressure acting area A is:

$$A = P^2 - \pi r_L^2 \tag{S8}$$

The breakthrough pressure P_{bk}: when the liquid reach the bottom, r_L=R, R is the base radius, which is half of pitch. The angle θ_A is the advancing contact angle.

$$P_L A + 2\pi r_L \gamma_{LV} \cos(\theta_A - \beta) = 0 \tag{S9}$$

$$P_{bk} = \frac{-\pi P \gamma_{LV} \cos(\theta_A - \beta)}{P^2 - P^2\pi/4} \tag{S10}$$

The robustness[2] A^* is defined as the ratio of breakthrough pressure P_{bk} and reference pressure P_{ref}. The P_{ref} is the liquid pressure with capillary length l_{cap} as radius.

$$A^* = \frac{P_{bk}}{\mathrm{P_{ref}}} \tag{S11}$$

$$\mathrm{P_{ref}} = \frac{2\gamma_{LV}}{l_{cap}} \tag{S12}$$

The contact angle data from experiment is plotted together with the modeling curve in FIG.5.

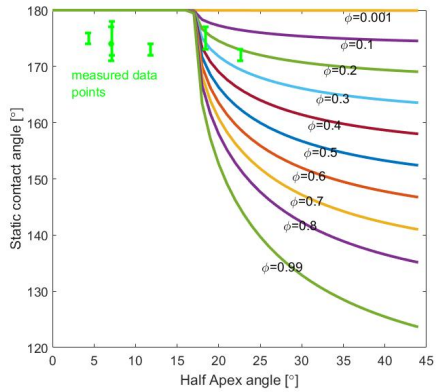

Fig. S. 5: Contact angle from experiment and model.

[1] D. Quéré, "Wetting and Roughness," Annual Review of Materials Research **38**, 71–99 (2008).
[2] A. Tuteja, W. Choi, J. M. Mabry, G. H. McKinley, and R. E. Cohen, "Robust omniphobic surfaces." Proceedings of the National Academy of Sciences of the United States of America **105**, 18200–5 (2008).

Chapter 4

Effect of micro-structures side wall and droplet impact velocity on Wenzel state droplet shape

Brief Summary

In this chapter, we investigate the effect of pillar lateral wall and droplet impact velocity on Wenzel state droplet shape. We produce various truncated cone surfaces and cylindrical pillar surfaces with the same top size, pitch and height but different lateral wall shape, namely conical shape or cylindrical shape. The change of lateral wall leads to change of the droplet shape using the same type of droplet. In addition, the droplet shape is also changed when increasing the Weber number, and the evolution of the droplet shape with the Weber number for truncated cone and cylindrical pillars is also different. This work advances the understanding of partial wetting drop shape, where the effect of the structure lateral wall shape and droplet deposition inertia is reported. The finding is meaningful and useful to various printing applications.

This chapter is under preparation and will be submitted to an international journal later.

Anisotropic wetting and final shape of droplets impacting on micropillars with non-vertical lateral walls

Wenwu Ding, Carlos Alberto Dorao, and Maria Fernandino*

Department of Energy and Process Engineering, Norwegian University of Science and Technology, 7491 Trondheim, Norway.

E-mail: maria.fernandino@ntnu.no

Phone: +47 73595352

Abstract

Control of droplet shape during impact on a solid surface is of relevance for several practical applications such as inkjet printing technologies. Although several studies have reported factors affecting the final droplet shape, understanding of the liquid spreading process is still lacking. In this work, droplets of different velocity are deposited on conical and cylindrical pillar surfaces. It is shown that for structures of the same height and pitch, the shape of the lateral wall of the micro-structures affects the droplet shape. In addition, at higher deposition velocity, the initial polygonal/square shape of the droplets evolves into a more circular shape. The change of shape due to the lateral wall of the structures is the result of the solid-liquid contact both above and below the structures and the way in which the liquid is able to move in between the structures for different passage area.

Chapter 5

Effect of microstructures sidewall topography on low surface tension drop impact

Brief Summary

In this chapter, we study the effect of conical structures sidewall topography on drop impact performance with varying surface tension. We produce conical surfaces with smooth sidewall and conical surfaces with re-entrant like lateral wall roughness. The latter structure looks like a tree-branch topography. By recording the drop impact process, we show that the conical structures mimicking a tree-branch like topography show enhanced anti-wetting ability. The critical Weber number showing partial rebound is higher for surfaces with sidewall roughness. Similar re-entrant like structures have been reported in literature either in modeling work or experimental work using random structures but no patterned base structures. Here we bridge the gap by using patterned structures with multi-layer re-entrant like sidewall roughness and reveal its effect.

This chapter is an article under preparation. It will be submitted to an international journal after some revisions, sometime during 2021.

Under Preparation

Improving superamphiphobicity by mimicking tree-branch topography

Wenwu Ding, Carlos Alberto Dorao, and Maria Fernandino*

Department of Energy and Process Engineering.

Norwegian University of Science and Technology

7491 Trondheim, Norway.

Abstract

When a droplet impacts a surface below a certain velocity, the droplet can bounce off completely from the structured surface. However, above such velocity a fraction of the droplet will pin on the surface. Surfaces capable of repelling water droplets are ubiquitous in nature or have been artificially fabricated. However, as the surface tension of the liquid is reduced, the capability of the surface to remain non-wetting gets hindered. Despite progress in previous research, the understanding and development of superamphiphobic surfaces for impacting of low surface tension droplets remains elusive. Here we show that conical microstructures mimicking tree-branches provide a surface topology capable of absorbing the force exerted by the droplet during the impact which prevents the droplet from pinning on the surface at higher impact velocities. Our study has significance for understanding the liquid interaction mechanism with the surface during the impact process and for the associated surface design considerations.

* maria.fernandino@ntnu.no.

Chapter 6

Effect of conical micro-pillars on water drop impact

Brief Summary

In this chapter, we study the role of conical micro-pillars on water drop impact behavior. We characterize the wetting properties and drop impact process. With the same pitch and height, the conical surfaces show higher contact angle, lower hysteresis, smaller receding time and higher number of bouncing, as compared to cylindrical pillars surfaces. But the critical Weber number is lower for conical case. However, the clean rebound at high Weber number can be achieved by optimization of the conical geometry. The drop residue size after impact is smaller for conical pillars when above the critical Weber number. We further record ethanol droplet behavior on the conical and cylindrical pillar surfaces with the same pitch and height, of which the results show that liquid inside cones is pinned while the liquid inside cylindrical case can move slowly. This behavior shows that the liquid mobility inside the cones is lower, thus impacting water droplets might wet less conical structures. This work shows that design of conical structures can help to maintain high contact angle, low hysteresis, high critical Weber number and smaller liquid residue size, which is a good pathway for achieving super-repellent performance.

This chapter is an article under preparation. It will be submitted to an international journal after some revisions, sometime during 2021.

Under Preparation

Effect of pillar side wall shape on water drop impact behavior

Wenwu Ding, Carlos Alberto Dorao, and Maria Fernandino*

Department of Energy and Process Engineering.

Norwegian University of Science and Technology

7491 Trondheim, Norway.

Abstract

Superhydrophobic surfaces are attractive due to their excellent water repellent performance. This can be achieved by designing the surface with nano- and micro-sized structures. A Cassie state droplet on such a superhydrophobic surface can show very high contact angle and low contact angle hysteresis with proper design. However, a transition from Cassie to Wenzel state occurs when a droplet impacts on the surface at high velocity. To achieve higher resistance to liquid impalement at the same scale, a dense array of structures or structures with pinning at the structures top are typically used, but with the sacrifice of increased contact angle hysteresis, which can lead to higher energy dissipation and lower number of droplet bouncings. In this work, micro-scale conical structures are adopted to achieve both low hysteresis and high anti-wetting ability. Comparing conical and cylindrical pillar structures with the same pitch and height, it is found that cylindrical pillars exhibit higher critical We number but at the same time result in larger contact angle hysteresis and larger liquid residue size when above a critical Weber number. By further reducing the apex angle of the conical structures, the anti-wetting ability of conical surfaces is improved. Therefore, a proper design of conical structures can maintain large contact angle, low hysteresis, strong resistance to impalement and higher number of bouncings. Even after penetration, the liquid residue size is small. In addition, the critical Weber number for the conical structures in this work is higher than for micro-patterned pillar surfaces found in the literature for the same pitch range, implying that we improve the anti-wetting performance further at the same structure scale.

* maria.fernandino@ntnu.no.

Chapter 7

Summary and outlook

7.1 Summary

The major contributions from this work are summarized below:

- Reveal the effect of conical geometry on surface static wetting properties, of which the cone apex angle is shown to play a major role.
- Report the effect of structures sidewall topography on Wenzel droplet shape at various impact velocities.
- Reveal the effect of sidewall roughness on low surface tension droplet impact behavior, which experimentally shows that the multi-layer re-entrant like sidewall roughness can enhance the anti-wetting performance.
- Reveal the effect of structures sidewall shape on water drop impact behavior. Conical surfaces have lower resistance to penetration but they show less wetted area when above a critical Weber number. Proper design of conical geometry can maintain high contact angle, low hysteresis, high number of bouncings and less liquid residue size, which means that conical structures are a nice candidate for anti-wetting purposes.
- Further develop and adapt the general lithography and etching recipe for producing conical structures [49] to fabricate various conical surfaces with both

smooth cones and cones with re-entrant like sidewall roughness.

In Chapter 3, we study how the conical geometry of microstructures can affect the static wetting properties of the surface. In this part, we use a force based model to relate conical geometry and its liquid penetration fraction, which is further related with the contact angle. It was revealed that the surface would be super-repellent for intrinsic contact angles larger than 90°. The conical half-apex angle plays an important role in suppressing the Cassie-Wenzel transition. This work provides more insight into conical microstructures effect on wetting properties. Furthermore, the results illustrate the prominent role of conical structures in achieving superhydrophobicity.

In Chapter 4, we investigate the role of microstructures sidewall shape in partial wetting drop pattern. To achieve this, we compare truncated conical pillars and cylindrical pillar surfaces and record from the top view to see how the drop shape evolves on these surfaces. In addition to pillar height/pitch and surface tension that have been shown to affect the droplet shape in previous work, we observe that the drop shape on truncated conical and cylindrical pillar surfaces is different even though they have the same pitch and height. Additionally, the drop shape at different impact Weber numbers is also evolving in different ways for truncated conical and cylindrical pillars. Based on the current results, it is concluded that the microstructures sidewall topography can play an important role in partial wetting drop shape.

In chapter 5, the effect of conical micro-pillars lateral wall topography on the surface anti-wetting properties is presented. In the literature, re-entrant shape like structures present Cassie state droplets for a wide range of surface tensions. It is reported that multi-layer re-entrant structures can further improve the anti-wetting performance in soft materials [68]. However, a partial Wenzel or Wenzel state droplet is still observed when the impact Weber number is increased. We fabricate tree-branch like conical structured surfaces and conduct drop impact experiments on these surfaces. It is shown that the tree-branch like structure does improve the anti-wetting performance by exhibiting a higher critical Weber number, compared with the smooth sidewall conical structures surfaces. The tree-branch like structures are able to reduce the solid-liquid contact but have higher resistance to penetration. As a result, this

type of topography enhances anti-wetting performance.

In Chapter 6, we study the effect of pillar sidewall shape on water drop impact dynamics at different Weber numbers. We further explore how the liquid residue size is affected, when the impact We lies above the critical Weber number for conical and cylindrical pillars. The conical micro-structured surfaces have higher contact angle and lower hysteresis whereas the cylindrical pillar case displays lower contact angle and higher hysteresis for the surfaces with small pitch arrays. At the same low Weber number $We \sim 2.8$, the bouncing height on conical structures is larger and with shorter receding time, which suggests that there is less energy loss in the case of conical structures. When the cylindrical and conical pillars have the same height and pitch, the conical pillars show lower critical Weber number as compared to cylindrical pillars. However, the liquid residue area on conical pillars (when the impact Weber number is above the critical value) is much smaller than for the cylindrical pillars case. This implies that the conical surfaces have less adhesion and wetted structure area. We found that this liquid residue size is affected by the We number, structure anti-penetration ability and liquid flow mobility inside the structure. Higher impact We number (when above the critical We number) means higher impact energy thus more liquid residue area can be observed. Stronger anti-penetration ability leads to less penetration and therefore less liquid residue area. Comparing an ethanol drop spreading on conical and cylindrical pillar surfaces with the same pitch and height, we observe that the liquid mobility within the cones is lower. We propose that the less liquid residue on the conical pillars case is partially due to the less wetted area owing to less open space within the cones. Along with decreased liquid residue size at high We number, the less energy dissipation for conical structures at low We number range further demonstrates the advantages of conical pillars shape in anti-wetting properties.

7.2 Outlook

From Chapter 3 to Chapter 6, we investigate the wetting properties of different structured surfaces with a focus on the effect of structures sidewall topography, in particular for conical pillars. However, there are still various things to be explored.

One possible future step is the direct imaging of the liquid-vapor interface on structured surfaces. This liquid-vapor interface can possibly be visualized by either environmental scanning electron microscope imaging [167, 168, 169], con-focal microscope imaging [170], or probably advanced neutron radiography[171] or X-ray imaging [172, 173, 174]. By direct imaging of the liquid-vapor interface on conical structures, the theoretic model can be further validated. For example, the actual liquid penetration depth and the liquid-vapor curvature there, which can deepen the physical understanding of the wetting phenomena.

Second, the conical structured surfaces here have high contact angle, low hysteresis and also favor Cassie wetting state with proper design, which makes them a good candidate for dewetting purposes in evaporation process. More work is thereby needed to study further how the structure sidewall shape plays a role in this dewetting process.

Third, the conical structured surfaces were shown to be a good candidate for condensation or fog collection process [56, 57, 58] as they favour certain directional droplet movement. Previously, this directional movement is explained to be driven by Laplace pressure gradient [51, 56, 57, 58]. But it is recently found that the Laplace pressure gradient is not the major player, rather it is the mismatch between the equilibrium contact angle and apparent contact angle which dominates the flow [55]. Therefore, it would be interesting to investigate how different conical pillars can affect the condensation or fog liquid movement dynamics further.

Bibliography

[1] Daniel Attinger, Christophe Frankiewicz, Amy R. Betz, Thomas M. Schutzius, Ranjan Ganguly, Arindam Das, Chang-Jin Kim, and Constantine M. Megaridis. Surface engineering for phase change heat transfer: A review. *MRS Energy & Sustainability*, 1:E4, 2014.

[2] Xi Yao, Qinwen Chen, Liang Xu, Qikai Li, Yanlin Song, Xuefeng Gao, David Quéré, and Lei Jiang. Bioinspired Ribbed Nanoneedles with Robust Superhydrophobicity. *Advanced Functional Materials*, 20(4):656–662, 2 2010.

[3] Kesong Liu and Lei Jiang. Bio-Inspired Self-Cleaning Surfaces. *Annual Review of Materials Research*, 42(1):231–263, 8 2012.

[4] Ralf Blossey. Self-cleaning surfaces — virtual realities. *Nature Materials*, 2(5):301–306, 5 2003.

[5] Yao Lu, Sanjayan Sathasivam, Jinlong Song, Colin R. Crick, Claire J. Carmalt, and Ivan P. Parkin. Robust self-cleaning surfaces that function when exposed to either air or oil. *Science*, 347(6226):1132–1135, 3 2015.

[6] Paul Calvert. Inkjet Printing for Materials and Devices. *Chemistry of Materials*, 13(10):3299–3305, 10 2001.

[7] John Kettle, Taina Lamminmäki, and Patrick Gane. A review of modified surfaces for high speed inkjet coating. *Surface and Coatings Technology*, 204(12-13):2103–2109, 3 2010.

[8] Shuoran Chen, Meng Su, Cong Zhang, Meng Gao, Bin Bao, Qiang Yang, Bin Su, and Yanlin Song. Fabrication of Nanoscale Circuits on Inkjet-Printing Patterned Substrates. *Advanced Materials*, 27(26):3928–3933, 7 2015.

[9] Berend-Jan de Gans and Ulrich S. Schubert. Inkjet Printing of Well-Defined Polymer Dots and Arrays. *Langmuir*, 20(18):7789–7793, 8 2004.

[10] Bong Kyun Park, Dongjo Kim, Sunho Jeong, Jooho Moon, and Jang Sub Kim. Direct writing of copper conductive patterns by ink-jet printing. *Thin Solid Films*, 515(19 SPEC. ISS.):7706–7711, 7 2007.

[11] Collin Ladd, Ju-Hee So, John Muth, and Michael D. Dickey. 3D Printing of Free Standing Liquid Metal Microstructures. *Advanced Materials*, 25(36):5081–5085, 9 2013.

[12] Qingbin Liu and Melissa Orme. High precision solder droplet printing technology and the state-of-the-art. *Journal of Materials Processing Technology*, 115(3):271–283, 9 2001.

[13] Q. Liu, M. C. Leu, and M. Orme. High precision solder droplet printing technology: Principle and applications. In *Proceedings of the International Symposium and Exhibition on Advanced Packaging Materials Processes, Properties and Interfaces*, pages 104–109, 2001.

[14] Xi Yao, Jun Gao, Yanlin Song, and Lei Jiang. Superoleophobic Surfaces with Controllable Oil Adhesion and Their Application in Oil Transportation. *Advanced Functional Materials*, 21(22):4270–4276, 11 2011.

[15] Chien-Chih Huang, Martin Z. Bazant, and Todd Thorsen. Ultrafast high-pressure AC electro-osmotic pumps for portable biomedical microfluidics. *Lab Chip*, 10(1):80–85, 1 2010.

[16] Roger Bodén, Klas Hjort, Jan-Åke Schweitz, and Urban Simu. A metallic micropump for high-pressure microfluidics. *Journal of Micromechanics and Microengineering*, 18(11):115009, 11 2008.

[17] William S.Y. Wong, Guanyu Liu, Noushin Nasiri, Chonglei Hao, Zuankai Wang, and Antonio Tricoli. Omnidirectional Self-Assembly of Transparent Superoleophobic Nanotextures. *ACS Nano*, 11(1):587–596, 2017.

[18] Shuaijun Pan, Arun K. Kota, Joseph M. Mabry, and Anish Tuteja. Superomniphobic Surfaces for Effective Chemical Shielding. *Journal of the American Chemical Society*, 135(2):578–581, 1 2013.

[19] Jiale Yong, Feng Chen, Qing Yang, Jinglan Huo, and Xun Hou. Superoleophobic surfaces. *Chemical Society Reviews*, 46(14):4168–4217, 7 2017.

[20] N. J. Shirtcliffe and P. Roach. Superhydrophobicity for Antifouling Microfluidic Surfaces. pages 269–281. Humana Press, Totowa, NJ, 2013.

[21] Xuemei Lu, Yuelian Peng, Haoran Qiu, Xinrui Liu, and Lei Ge. Anti-fouling membranes by manipulating surface wettability and their anti-fouling mechanism. *Desalination*, 413:127–135, 7 2017.

[22] Ziqi Sun, Ting Liao, Kesong Liu, Lei Jiang, Jung Ho Kim, and Shi Xue Dou. Fly-Eye Inspired Superhydrophobic Anti-Fogging Inorganic Nanostructures. *Small*, 10(15):3001–3006, 8 2014.

[23] Mingjie Liu, Shutao Wang, and Lei Jiang. Nature-inspired superwettability systems. *Nature Reviews Materials*, 2(7):17036, 7 2017.

[24] Jeong-Gil Kim, Hyungryul J. Choi, Kyoo-Chul Park, Robert E. Cohen, Gareth H. McKinley, and George Barbastathis. Multifunctional Inverted Nanocone Arrays for Non-Wetting, Self-Cleaning Transparent Surface with High Mechanical Robustness. *Small*, 10(12):2487–2494, 6 2014.

[25] Liangliang Cao, Andrew K. Jones, Vinod K. Sikka, Jianzhong Wu, and Di Gao. Anti-Icing Superhydrophobic Coatings. *Langmuir*, 25(21):12444–12448, 11 2009.

[26] Peng Guo, Yongmei Zheng, Mengxi Wen, Cheng Song, Yucai Lin, and Lei Jiang. Icephobic/Anti-Icing Properties of Micro/Nanostructured Surfaces. *Advanced Materials*, 24(19):2642–2648, 5 2012.

[27] Xuemei Chen, Justin A. Weibel, and Suresh V. Garimella. Exploiting Microscale Roughness on Hierarchical Superhydrophobic Copper Surfaces for Enhanced Dropwise Condensation. *Advanced Materials Interfaces*, 2(3):1400480, 2 2015.

[28] Xuemei Chen, Jun Wu, Ruiyuan Ma, Meng Hua, Nikhil Koratkar, Shuhuai Yao, and Zuankai Wang. Nanograssed Micropyramidal Architectures for Continuous Dropwise Condensation. *Advanced Functional Materials*, 21(24):4617–4623, 12 2011.

[29] Nenad Miljkovic, Ryan Enright, Youngsuk Nam, Ken Lopez, Nicholas Dou, Jean Sack, and Evelyn N. Wang. Jumping-Droplet-Enhanced Condensation on Scalable Superhydrophobic Nanostructured Surfaces. *Nano Letters*, 13(1):179–187, 1 2013.

[30] Konrad Rykaczewski, Adam T. Paxson, Matthew Staymates, Marlon L. Walker, Xiaoda Sun, Sushant Anand, Siddarth Srinivasan, Gareth H. McKinley, Jeff Chinn, John Henry J. Scott, and Kripa K. Varanasi. Dropwise condensation of low surface tension fluids on omniphobic surfaces. *Scientific Reports*, 4(1):1–8, 3 2014.

[31] Melanie M. Derby, Allison N. Adams, Partha P. Chakraborty, Mohammad Rejaul Haque, Ryan A. Huber, Jordan A. Morrow, Gennifer A. Riley, Molly Ross, Emily M. Stallbaumer, Amy R. Betz, and Hitesh Bindra. Heat and Mass Transfer in the Food, Energy, and Water Nexus—A Review. *Journal of Heat Transfer*, 142(9):90801–90802, 9 2020.

[32] Christof Sodtke and Peter Stephan. Spray cooling on micro structured surfaces. *International Journal of Heat and Mass Transfer*, 50(19-20):4089–4097, 9 2007.

[33] Jian Nan Chen, Zhen Zhang, Rui Na Xu, Xiao Long Ouyang, and Pei Xue Jiang. Numerical Investigation of the Flow Dynamics and Evaporative Cooling of Water Droplets Impinging onto Heated Surfaces: An Effective Approach to Identify Spray Cooling Mechanisms. *Langmuir*, 32(36):9135–9155, 9 2016.

[34] S. David, K. Sefiane, and L. Tadrist. Experimental investigation of the effect of thermal properties of the substrate in the wetting and evaporation of sessile drops. *Colloids and Surfaces A: Physicochemical and Engineering Aspects*, 298(1-2):108–114, 2007.

[35] Sera Shin, Jungmok Seo, Heetak Han, Subin Kang, Hyunchul Kim, and Taeyoon Lee. Bio-inspired extreme wetting surfaces for biomedical applications, 2 2016.

[36] Hans J Ensikat, Petra Ditsche-Kuru, Christoph Neinhuis, Wilhelm Barthlott, Guest Editors, W Barthlott, and K Koch. Superhydrophobicity in perfection: the outstanding properties of the lotus leaf. *Beilstein J. Nanotechnol*, 2:152–161, 2011.

[37] Seung Goo Lee, Ho Sun Lim, Dong Yun Lee, Donghoon Kwak, and Kilwon Cho. Tunable Anisotropic Wettability of Rice Leaf-Like Wavy Surfaces. *Advanced Functional Materials*, 23(5):547–553, 2 2013.

[38] Jia Yao, Jian Nan Wang, Yan Hao Yu, Han Yang, and Ying Xu. Biomimetic fabrication and characterization of an artificial rice leaf surface with anisotropic wetting. *Chinese Science Bulletin*, 57(20):2631–2634, 7 2012.

[39] Yan Fang, Gang Sun, Tong Qing Wang, Qian Cong, and Lu Quan Ren. Hydrophobicity mechanism of non-smooth pattern on surface of butterfly wing. *Chinese Science Bulletin*, 52(5):711–716, 3 2007.

[40] Gang Sun, Yan Fang, Qian Cong, and Lu quan Ren. Anisotropism of the Non-Smooth Surface of Butterfly Wing. *Journal of Bionic Engineering*, 6(1):71–76, 3 2009.

[41] Andrew R. Parker and Chris R. Lawrence. Water capture by a desert beetle. *Nature*, 414(6859):33–34, 11 2001.

[42] H. Yildirim Erbil. The debate on the dependence of apparent contact angles on drop contact area or three-phase contact line: A review. *Surface Science Reports*, 69(4):325–365, 2014.

[43] Hao Wang. From Contact Line Structures to Wetting Dynamics. *Langmuir*, 35(32):10233–10245, 8 2019.

[44] Daniel Bonn, Jens Eggers, Joseph Indekeu, and Jacques Meunier. Wetting and spreading. *Reviews of Modern Physics*, 81(2):739–805, 5 2009.

[45] Eiji Hosono, Shinobu Fujihara, Itaru Honma, and Haoshen Zhou. Superhydrophobic perpendicular nanopin film by the bottom-up process. *Journal of the American Chemical Society*, 127(39):13458–13459, 10 2005.

[46] Elena Martines, Kris Seunarine, Hywel Morgan, Nikolaj Gadegaard, Chris D.W. Wilkinson, and Mathis O. Riehle. Superhydrophobicity and superhydrophilicity of regular nanopatterns. *Nano Letters*, 5(10):2097–2103, 2005.

[47] Timothée Mouterde, Gaëlle Lehoucq, Stéphane Xavier, Antonio Checco, Charles T. Black, Atikur Rahman, Thierry Midavaine, Christophe Clanet, and David Quéré. Antifogging abilities of model nanotextures. *Nature Materials*, 16(6):658–663, 2017.

[48] Agnieszka Telecka, Tao Li, Sokol Ndoni, and Rafael Taboryski. Nanotextured Si surfaces derived from block-copolymer self-assembly with superhydrophobic, superhydrophilic, or superamphiphobic properties. *RSC Advances*, 8(8):4204–4213, 2018.

[49] I W Park, Maria Fernandino, and C A Dorao. Wetting State Transitions over Hierarchical Conical Microstructures. *Advanced Materials Interfaces*, 2018.

[50] Chander Shekhar Sharma, Christos Stamatopoulos, Reto Suter, Philipp Rudolf von Rohr, and Dimos Poulikakos. Rationally 3D-Textured Copper Surfaces for Laplace Pressure Imbalance-Induced Enhancement in Dropwise Condensation. *ACS Applied Materials & Interfaces*, 10(34):29127–29135, 8 2018.

[51] Élise Lorenceau and David Quéré. Drops on a conical wire. *J. Fluid Mech*, 510:29–45, 2004.

[52] Yongmei Zheng, Hao Bai, Zhongbing Huang, Xuelin Tian, Fu Qiang Nie, Yong Zhao, Jin Zhai, and Lei Jiang. Directional water collection on wetted spider silk. *Nature*, 463(7281):640–643, 2010.

[53] Bo Zhang, Xuemei Chen, Jure Dobnikar, Zuankai Wang, and Xianren Zhang. Spontaneous Wenzel to Cassie dewetting transition on structured surfaces. *Physical Review Fluids*, 1(7):1–11, 2016.

[54] Yong Jin, Adnan Qamar, Yusuf Shi, and Peng Wang. Preferential water condensation on superhydrophobic nano-cones array. *Applied Physics Letters*, 113(21), 2018.

[55] Tak Shing Chan, Fan Yang, and Andreas Carlson. Directional spreading of a viscous droplet on a conical fibre. *Journal of Fluid Mechanics*, 894:26, 2020.

[56] Charles T. Schriner and Bharat Bhushan. Water droplet dynamics on bioinspired conical surfaces. *Philosophical Transactions of the Royal Society A: Mathematical, Physical and Engineering Sciences*, 377(2150), 2019.

[57] Hui Zhou, Xueshan Jing, and Zhiguang Guo. Optimal Design of a Fog Collector: Unidirectional Water Transport on a System Integrated by Conical Copper Needles with Gradient Wettability and Hydrophilic Slippery Rough Surfaces. *Langmuir*, 36(24):6801–6810, 6 2020.

[58] Dev Gurera and Bharat Bhushan. Multistep Wettability Gradient on Bioinspired Conical Surfaces for Water Collection from Fog. *Langmuir*, 35(51):16944–16947, 12 2019.

[59] Thomas Young. III. An essay on the cohesion of fluids. *Philosophical Transactions of the Royal Society of London*, 95:65–87, 1 1805.

[60] A. B.D. Cassie and S. Baxter. Wettability of porous surfaces. *Transactions of the Faraday Society*, 40:546–551, 1944.

[61] José Bico, Uwe Thiele, and David Quéré. Wetting of textured surfaces. *Colloids and Surfaces A: Physicochemical and Engineering Aspects*, 206(1-3):41–46, 2002.

[62] Adrien Bussonnière, Masoud B. Bigdeli, Di Yen Chueh, Qingxia Liu, Peilin Chen, and Peichun Amy Tsai. Universal wetting transition of an evaporating water droplet on hydrophobic micro- and nano-structures. *Soft Matter*, 13(5):978–984, 2 2017.

[63] Yanshen Li, David Quéré, Cunjing Lv, and Quanshui Zheng. Monostable superrepellent materials. *Proceedings of the National Academy of Sciences*, 114(13):3387–3392, 2017.

[64] W. Ding, M. Fernandino, and C. A. Dorao. Conical micro-structures as a route for achieving super-repellency in surfaces with intrinsic hydrophobic properties. *Applied Physics Letters*, 115(5):053703, 7 2019.

[65] Yan Liu, Xinlin Li, Jingfu Jin, Jiaan Liu, Yuying Yan, Zhiwu Han, and Luquan Ren. Anti-icing property of bio-inspired micro-structure superhydrophobic surfaces and heat transfer model. *Applied Surface Science*, 400:498–505, 2017.

[66] P. Joseph, C. Cottin-Bizonne, J. M. Benoît, C. Ybert, C. Journet, P. Tabeling, and L. Bocquet. Slippage of water past superhydrophobic carbon nanotube forests in microchannels. *Physical Review Letters*, 97(15):1–4, 2006.

[67] A. Tuteja, W. Choi, J. M. Mabry, G. H. McKinley, and R. E. Cohen. Robust omniphobic surfaces. *Proceedings of the National Academy of Sciences*, 105(47):18200–18205, 2008.

[68] Shuaijun Pan, Rui Guo, Mattias Björnmalm, Joseph J. Richardson, Ling Li, Chang Peng, Nadja Bertleff-Zieschang, Weijian Xu, Jianhui Jiang, and Frank Caruso. Coatings super-repellent to ultralow surface tension liquids. *Nature Materials*, 17(11):1040–1047, 11 2018.

[69] James C. Bird, Rajeev Dhiman, Hyuk Min Kwon, and Kripa K. Varanasi. Reducing the contact time of a bouncing drop. *Nature*, 503(7476):385–388, 2013.

[70] B D'Urso, J T Simpson, and M Kalyanaraman. Emergence of superhydrophobic behavior on vertically aligned nanocone arrays. *Appl. Phys. Lett.*, 90(4):N.PAG, 2007.

[71] Jun De Li. CFD simulation of water vapour condensation in the presence of non-condensable gas in vertical cylindrical condensers. *International Journal of Heat and Mass Transfer*, 57(2):708–721, 2013.

[72] Antonio Checco, Benjamin M. Ocko, Atikur Rahman, Charles T. Black, Mykola Tasinkevych, Alberto Giacomello, and Siegfried Dietrich. Collapse and reversibility of the superhydrophobic state on nanotextured surfaces. *Physical Review Letters*, 112(21):1–5, 2014.

[73] Katrina M. Wisdom, Jolanta A. Watson, Xiaopeng Qu, Fangjie Liu, Gregory S. Watson, and Chuan Hua Chen. Self-cleaning of superhydrophobic surfaces by self-propelled jumping condensate. *Proceedings of the National Academy of Sciences of the United States of America*, 110(20):7992–7997, 5 2013.

[74] Kyoo Chul Park, Hyungryul J. Choi, Chih Hao Chang, Robert E. Cohen, Gareth H. McKinley, and George Barbastathis. Nanotextured silica surfaces with robust superhydrophobicity and omnidirectional broadband supertransmissivity. *ACS Nano*, 6(5):3789–3799, 2012.

[75] Rishi Raj, Solomon Adera, Ryan Enright, and Evelyn N. Wang. High-resolution liquid patterns via three-dimensional droplet shape control. *Nature Communications*, 5(1):4975, 12 2014.

[76] Yong Chen, Bo He, Junghoon Lee, and Neelesh A. Patankar. Anisotropy in the wetting of rough surfaces. *Journal of Colloid and Interface Science*, 281(2):458–464, 1 2005.

[77] Jun Young Chung, Jeffrey P. Youngblood, and Christopher M. Stafford. Anisotropic wetting on tunable micro-wrinkled surfaces. *Soft Matter*, 3(9):1163–1169, 8 2007.

[78] Yan Zhao, Qinghua Lu, Mei Li, and Xin Li. Anisotropic wetting characteristics on submicrometer-scale periodic grooved surface. *Langmuir*, 23(11):6212–6217, 5 2007.

[79] H. Kusumaatmaja, R. J. Vrancken, C. W.M. Bastiaansen, and J. M. Yeomans. Anisotropic drop morphologies on corrugated surfaces. *Langmuir*, 24(14):7299–7308, 7 2008.

[80] Wen Li, Guoping Fang, Yongfeng Li, and Guanjun Qiao. Anisotropic wetting behavior arising from superhydrophobic surfaces: Parallel grooved structure. *Journal of Physical Chemistry B*, 112(24):7234–7243, 6 2008.

[81] Lu Tie, Zhiguang Guo, and Weimin Liu. Anisotropic wetting properties on various shape of parallel grooved microstructure. *Journal of Colloid and Interface Science*, 453:142–150, 9 2015.

[82] T. Cubaud and M. Fermigier. Faceted drops on heterogeneous surfaces. *EPL (Europhysics Letters)*, 55(2):239, 2001.

[83] Laurent Courbin, Etienne Denieul, Emilie Dressaire, Marcus Roper, Armand Ajdari, and Howard A. Stone. Imbibition by polygonal spreading on microdecorated surfaces. *Nature Materials*, 6(9):661–664, 9 2007.

[84] Robert J. Vrancken, Matthew L. Blow, Halim Kusumaatmaja, Ko Hermans, An M. Prenen, Cees W. M. Bastiaansen, Dirk J. Broer, and Julia M. Yeomans. Anisotropic wetting and de-wetting of drops on substrates patterned with polygonal posts. *Soft Matter*, 9(3):674–683, 12 2013.

[85] Huicheng Feng, Karen Siew-Ling Chong, Kian-Soo Ong, and Fei Duan. Octagon to Square Wetting Area Transition of Water–Ethanol Droplets on a Micropyramid Substrate by Increasing Ethanol Concentration. *Langmuir*, 33(5):1147–1154, 2 2017.

[86] Xin Zhong, Junheng Ren, Mingfeng Lin, Karen Siew Ling Chong, Kian-Soo Ong, and Fei Duan. Octagonal Wetting Interface Evolution of Evaporating Saline Droplets on a Micropyramid Patterned Surface. *ACS Applied Materials & Interfaces*, 9(33):28055–28063, 8 2017.

[87] Enhui Chen, Quanzi Yuan, Xianfu Huang, and Ya-Pu Zhao. Dynamic polygonal spreading of a droplet on a lyophilic pillar-arrayed surface. *Journal of Adhesion Science and Technology*, 30(20):2265–2276, 10 2016.

[88] Alok Kumar and Rishi Raj. Droplets on Microdecorated Surfaces: Evolution of the Polygonal Contact Line. *Langmuir*, 33(19):4854–4862, 5 2017.

[89] M. L. Blow and J. M. Yeomans. Anisotropic imbibition on surfaces patterned with polygonal posts. *Philosophical Transactions of the Royal Society A: Mathematical, Physical and Engineering Sciences*, 369(1945):2519–2527, 6 2011.

[90] Qian Zhang, Tie Zheng Qian, and Xiao Ping Wang. Phase field simulation of a droplet impacting a solid surface. *Physics of Fluids*, 28(2):022103, 2 2016.

[91] Arnoldo Badillo. Quantitative phase-field modeling for wetting phenomena. *Physical Review E - Statistical, Nonlinear, and Soft Matter Physics*, 91(3):033005, 3 2015.

[92] Petter Johansson, Andreas Carlson, and Berk Hess. Water-substrate physicochemistry in wetting dynamics. *Journal of Fluid Mechanics*, 781:695–711, 2015.

[93] Jungchul Kim, Myoung-Woon Moon, and Ho-Young Kim. Dynamics of hemiwicking. *J. Fluid Mech*, 800:57–71, 2016.

[94] Hyoungsoo Kim, Zhong Zheng, and Howard A. Stone. Noncircular stable displacement patterns in a meshed porous layer. *Langmuir*, 31(20):5684–5688, 5 2015.

[95] D. Sivakumar, K. Katagiri, T. Sato, and H. Nishiyama. Spreading behavior of an impacting drop on a structured rough surface. *Physics of Fluids*, 17(10):100608, 10 2005.

[96] Songlin Shi, Songlin Shi, Cunjing Lv, Cunjing Lv, Quanshui Zheng, Quanshui Zheng, and Quanshui Zheng. Temperature-regulated adhesion of impacting drops on nano/microtextured monostable superrepellent surfaces. *Soft Matter*, 16(23):5388–5397, 2020.

[97] A.L. Yarin. Drop impact dynamics: Splashing, Spreading, Receding, Bouncing.... *Annual Review of Fluid Mechanics*, 38(1):159–192, 1 2006.

[98] R. Rioboo, M. Marengo, and C. Tropea. Time evolution of liquid drop impact onto solid, dry surfaces. *Experiments in Fluids*, 33(1):112–124, 2002.

[99] Hyungmo Kim, Chan Lee, Moo Hwan Kim, and Joonwon Kim. Drop impact characteristics and structure effects of hydrophobic surfaces with micro-and/or nanoscaled structures. *Langmuir*, 28(30):11250–11257, 7 2012.

[100] C. Josserand and S.T. Thoroddsen. Drop Impact on a Solid Surface. *Annual Review of Fluid Mechanics*, 48(1):365–391, 1 2016.

[101] Jolet De Ruiter, Rudy Lagraauw, Dirk Van Den Ende, and Frieder Mugele. Wettability-independent bouncing on flat surfaces mediated by thin air films. *Nature Physics*, 11(1):48–53, 1 2015.

[102] ILKER S. BAYER and CONSTANTINE M. MEGARIDIS. Contact angle dynamics in droplets impacting on flat surfaces with different wetting characteristics. *Journal of Fluid Mechanics*, 558:415, 7 2006.

[103] M Pasandideh-Fard, Y M Qiao, S Chandra, and J Mostaghimi. Capillary effects during droplet impact on a solid surface. *Physics of Fluids*, 8:650, 1996.

[104] Xu Deng, Frank Schellenberger, Periklis Papadopoulos, Doris Vollmer, and Hans Jürgen Butt. Liquid drops impacting superamphiphobic coatings. *Langmuir*, 29(25):7847–7856, 2013.

[105] Carlo Antonini, Alidad Amirfazli, and Marco Marengo. Drop impact and wettability: From hydrophilic to superhydrophobic surfaces. *Physics of Fluids*, 24(10), 2012.

[106] C. Antonini, F. Villa, I. Bernagozzi, A. Amirfazli, and M. Marengo. Drop Rebound after Impact: The Role of the Receding Contact Angle. *Langmuir*, 29(52):16045–16050, 12 2013.

[107] Ileana Malavasi, Federico Veronesi, Aurora Caldarelli, Maurizio Zani, Mariarosa Raimondo, and Marco Marengo. Is a Knowledge of Surface Topology and Contact Angles Enough to Define the Drop Impact Outcome? *Langmuir*, 32(25):6255–6262, 6 2016.

[108] Z. Wang, C. Lopez, A. Hirsa, and N. Koratkar. Impact dynamics and rebound of water droplets on superhydrophobic carbon nanotube arrays. *Applied Physics Letters*, 91(2), 2007.

[109] M. Reyssat, A. Pépin, F. Marty, Y. Chen, and D. Quéré. Bouncing transitions on microtextured materials. *Europhysics Letters*, 74(2):306–312, 2006.

[110] D. Bartolo, F. Bouamrirene, É Verneuil, A. Buguin, P. Silberzan, and S. Moulinet. Bouncing or sticky droplets: Impalement transitions on superhydrophobic micropatterned surfaces. *Europhysics Letters*, 74(2):299–305, 2006.

[111] Yang Xu. *Normal impact of liquid droplets on smooth solid surfaces*. PhD thesis, Université Paris-Est, 2018.

[112] Andreas Carlson, Minh Do-Quang, and Gustav Amberg. Modeling of dynamic wetting far from equilibrium, 12 2009.

[113] A. Carlson, M. Do-Quang, and G. Amberg. Dissipation in rapid dynamic wetting. *Journal of Fluid Mechanics*, 682:213–240, 9 2011.

[114] A. Carlson, G. Bellani, and G. Amberg. Contact line dissipation in short-time dynamic wetting. *EPL*, 97(4):44004, 2 2012.

[115] Andreas Carlson, Gabriele Bellani, and Gustav Amberg. Universality in dynamic wetting dominated by contact-line friction. *Physical Review E - Statistical, Nonlinear, and Soft Matter Physics*, 85(4):045302, 4 2012.

[116] Yoshinori Nakamura, Andreas Carlson, Gustav Amberg, and Junichiro Shiomi. Dynamic wetting at the nanoscale. *Physical Review E - Statistical, Nonlinear, and Soft Matter Physics*, 88(3):033010, 9 2013.

[117] Yuli Wang, Gustav Amberg, and Andreas Carlson. Local dissipation limits the dynamics of impacting droplets on smooth and rough substrates. *Physical Review Fluids*, 2(3):033602, 3 2017.

[118] Yu Xu, Xiande Fang, Xianghui Su, Zhanru Zhou, and Weiwei Chen. Evaluation of frictional pressure drop correlations for two-phase flow in pipes. *Nuclear Engineering and Design*, 253:86–97, 12 2012.

[119] Ted Mao, David C.S. Kuhn, and Honghi Tran. Spread and Rebound of Liquid Droplets upon Impact on Flat Surfaces. *AIChE Journal*, 43(9):2169–2179, 1997.

[120] R Rioboo, M Marengo, and C Tropea. Time evolution of liquid drop impact onto solid, dry surfaces. *Experiments in Fluids*, 33:112–124, 2002.

[121] D. Richard and D. Quéré. Bouncing water drops. *Europhysics Letters*, 50(6):769–775, 2000.

[122] Anne-Laure Biance and Guillaume Lagubeau. On the Elasticity of an Inertial Liquid Shock. *Journal of Fluid Mechanics*, 554:47–66, 2006.

[123] Christophe Clanet. Water Spring : A Model for Bouncing Drops. *Europhys. Lett.*, 62(December):237–243, 2002.

[124] R. Rioboo, M. Voue´, A. Vaillant, and J. De Coninck. Drop Impact on Porous Superhydrophobic Polymer Surfaces. *Langmuir*, 24(24):14074–14077, 12 2008.

[125] Kosmas Ellinas, Marianneza Chatzipetrou, Ioanna Zergioti, Angeliki Tserepi, and Evangelos Gogolides. Superamphiphobic Polymeric Surfaces Sustaining Ultrahigh Impact Pressures of Aqueous High- and Low-Surface-Tension Mixtures, Tested with Laser-Induced Forward Transfer of Drops. *Advanced Materials*, 27(13):2231–2235, 4 2015.

[126] Lei Xu, Wendy W. Zhang, and Sidney R. Nagel. Drop splashing on a dry smooth surface. *Physical Review Letters*, 94(18):184505, 5 2005.

[127] Yisen Guo, Yongsheng Lian, and Mark Sussman. Investigation of drop impact on dry and wet surfaces with consideration of surrounding air. *Physics of Fluids*, 28(7):73303, 7 2016.

[128] Shreyas Mandre, Madhav Mani, and Michael P. Brenner. Precursors to splashing of liquid droplets on a solid surface. *Physical Review Letters*, 102(13):134502, 3 2009.

[129] Michelle M. Driscoll and Sidney R. Nagel. Ultrafast interference imaging of air in splashing dynamics. *Physical Review Letters*, 107(15):154502, 10 2011.

[130] Roeland C.A. Van Der Veen, Tuan Tran, Detlef Lohse, and Chao Sun. Direct measurements of air layer profiles under impacting droplets using high-speed color interferometry. *Physical Review E - Statistical, Nonlinear, and Soft Matter Physics*, 85(2):026315, 2 2012.

[131] John M. Kolinski, Shmuel M. Rubinstein, Shreyas Mandre, Michael P. Brenner, David A. Weitz, and L. Mahadevan. Skating on a film of air: Drops impacting on a surface. *Physical Review Letters*, 108(7):074503, 2 2012.

[132] Ji San Lee, Byung Mook Weon, Jung Ho Je, and Kamel Fezzaa. How does an air film evolve into a bubble during drop impact? *Physical Review Letters*, 109(20):204501, 11 2012.

[133] Roeland C.A. Van Der Veen, Maurice H.W. Hendrix, Tuan Tran, Chao Sun, Peichun Amy Tsai, and Detlef Lohse. How microstructures affect air film dynamics prior to drop impact. *Soft Matter*, 10(21):3703–3707, 6 2014.

[134] Minori Shirota, Michiel A.J. van Limbeek, Detlef Lohse, and Chao Sun. Measuring thin films using quantitative frustrated total internal reflection (FTIR). *European Physical Journal E*, 40(5):54, 5 2017.

[135] Evert Klaseboer, Rogerio Manica, and Derek Y.C. Chan. Universal behavior of the initial stage of drop impact. *Physical Review Letters*, 113(19):194501, 11 2014.

[136] Peichun Tsai, Maurice H.W. Hendrix, Remko R.M. Dijkstra, Lingling Shui, and Detlef Lohse. Microscopic structure influencing macroscopic splash at high Weber number. *Soft Matter*, 7(24):11325–11333, 12 2011.

[137] Kenneth R. Langley, Er Qiang Li, Ivan U. Vakarelski, and Sigurdur T. Thoroddsen. The air entrapment under a drop impacting on a nano-rough surface. *Soft Matter*, 14(37):7586–7596, 9 2018.

[138] Longquan Chen, Long Li, Zhigang Li, and Kai Zhang. Submillimeter-Sized Bubble Entrapment and a High-Speed Jet Emission during Droplet Impact on Solid Surfaces. *Langmuir*, 33(29):7225–7230, 7 2017.

[139] Susmita Dash, Marie T. Alt, and Suresh V. Garimella. Hybrid Surface Design for Robust Superhydrophobicity. *Langmuir*, 28(25):9606–9615, 6 2012.

[140] Katherine Smyth, Adam Paxon, Hyuk-min Kwon, Tao Deng, and Kripa K. Varanasi. Dynamic wetting on superhydrophobic surfaces: Droplet impact and wetting hysteresis. In *2010 12th IEEE Intersociety Conference on Thermal and Thermomechanical Phenomena in Electronic Systems*, pages 1–8. IEEE, 6 2010.

[141] Nagesh D. Patil, Rajneesh Bhardwaj, and Atul Sharma. Droplet impact dynamics on micropillared hydrophobic surfaces. *Experimental Thermal and Fluid Science*, 74:195–206, 2016.

[142] Laxman K. Malla, Nagesh D. Patil, Rajneesh Bhardwaj, and Adrian Neild. Droplet Bouncing and Breakup during Impact on a Microgrooved Surface. *Langmuir*, 33(38):9620–9631, 2017.

[143] Yong Chae Jung and Bharat Bhushan. Dynamic effects of bouncing water droplets on superhydrophobic surfaces. *Langmuir*, 24(12):6262–6269, 2008.

[144] C. Frankiewicz and D. Attinger. Texture and wettability of metallic lotus leaves. *Nanoscale*, 8(7):3982–3990, 2 2016.

[145] S. Moulinet and D. Bartolo. Life and death of a fakir droplet: Impalement transitions on superhydrophobic surfaces. *European Physical Journal E*, 24(3):251–260, 2007.

[146] Anish Tuteja, Wonjae Choi, Minglin Ma, Joseph M Mabry, Sarah A Mazzella, Gregory C Rutledge, Gareth H McKinley, and Robert E Cohen. Designing superoleophobic surfaces. *Science (New York, N.Y.)*, 318(5856):1618–22, 12 2007.

[147] A. Tuteja, W. Choi, M. Ma, J. M. Mabry, S. A. Mazzella, G. C. Rutledge, G. H. McKinley, and R. E. Cohen. Designing Superoleophobic Surfaces. *Science*, 318(5856):1618–1622, 11 2014.

[148] Bo Zhang and Xianren Zhang. Elucidating Nonwetting of Re-Entrant Surfaces with Impinging Droplets. *Langmuir*, 31(34):9448–9457, 2015.

[149] Gene Whyman and Edward Bormashenko. How to make the cassie wetting state stable? *Langmuir*, 27(13):8171–8176, 2011.

[150] Hans Jürgen Butt, Ciro Semprebon, Periklis Papadopoulos, Doris Vollmer, Martin Brinkmann, and Matteo Ciccotti. Design principles for superamphiphobic surfaces. *Soft Matter*, 9(2):418–428, 1 2013.

[151] René Hensel, Ralf Helbig, Sebastian Aland, Hans Georg Braun, Axel Voigt, Christoph Neinhuis, and Carsten Werner. Wetting resistance at its topographical limit: The benefit of mushroom and serif T structures. *Langmuir*, 29(4):1100–1112, 1 2013.

[152] C. Frankiewicz and D. Attinger. Texture and wettability of metallic lotus leaves. *Nanoscale*, 8(7):3982–3990, 2 2016.

[153] Seunghyeon Baek, Hyun Sik Moon, Wuseok Kim, Sangmin Jeon, and Kijung Yong. Effect of liquid droplet surface tension on impact dynamics over hierarchical nanostructure surfaces. *Nanoscale*, 10(37):17842–17851, 9 2018.

[154] Matthew McCarthy, Konstantinos Gerasopoulos, Ryan Enright, James N. Culver, Reza Ghodssi, and Evelyn N. Wang. Biotemplated hierarchical surfaces and the role of dual length scales on the repellency of impacting droplets. *Applied Physics Letters*, 100(26):263701, 6 2012.

[155] Neelesh A. Patankar. Consolidation of Hydrophobic Transition Criteria by Using an Approximate Energy Minimization Approach. *Langmuir*, 26(11):8941–8945, 6 2010.

[156] James Jurin. An account of some experiments shown before the Royal Society; with an enquiry into the cause of the ascent and suspension of water in capillary tubes. *Philosophical Transactions of the Royal Society of London*, 30(355):739–747, 12 1719.

[157] J. Hyväluoma and J. Timonen. Impact states and energy dissipation in bouncing and non-bouncing droplets. *Journal of Statistical Mechanics: Theory and Experiment*, 2009(6):P06010, 6 2009.

[158] Philip S. Brown and Bharat Bhushan. Durable, superoleophobic polymer–nanoparticle composite surfaces with re-entrant geometry via solvent-induced phase transformation. *Scientific Reports*, 6(1):21048, 8 2016.

[159] Xuemei Chen, Justin A. Weibel, and Suresh V. Garimella. Characterization of Coalescence-Induced Droplet Jumping Height on Hierarchical Superhydrophobic Surfaces. *ACS Omega*, 2(6):2883–2890, 2017.

[160] Yi Wu, Jing Zeng, Yinsong Si, Min Chen, and Limin Wu. Large-Area Preparation of Robust and Transparent Superomniphobic Polymer Films. *ACS Nano*, 12(10):10338–10346, 2018.

[161] Min Xi, Jiale Yong, Feng Chen, Qing Yang, and Xun Hou. A femtosecond laser-induced superhygrophobic surface: beyond superhydrophobicity and repelling various complex liquids. *RSC Advances*, 9(12):6650–6657, 2 2019.

[162] Hyunchul Kim, Heetak Han, Sanggeun Lee, Janghoon Woo, Jungmok Seo, and Taeyoon Lee. Nonfluorinated Superomniphobic Surfaces through Shape-Tunable Mushroom-like Polymeric Micropillar Arrays. *ACS Applied Materials and Interfaces*, 11(5):5484–5491, 2 2019.

[163] Shuantao Dong, Yabin Li, Ning Tian, Bucheng Li, Yanfei Yang, Lingxiao Li, and Junping Zhang. Scalable Preparation of Superamphiphobic Coatings with Ultralow Sliding Angles and High Liquid Impact Resistance. *ACS Applied Materials and Interfaces*, 10(49):41878–41882, 12 2018.

[164] William S.Y. Wong. Surface Chemistry Enhancements for the Tunable Super-Liquid Repellency of Low-Surface-Tension Liquids. *Nano Letters*, 19(3):1892–1901, 3 2019.

[165] William S.Y. Wong. Surface Chemistry Enhancements for the Tunable Super-Liquid Repellency of Low-Surface-Tension Liquids. *Nano Letters*, 19(3):1892–1901, 2019.

[166] A J Wheeler and A R Ganji. *Introduction to Engineering Experimentation.* New Jersey: Prentice Hall, 1996.

[167] HangJin Jo, Kyung Won Hwang, DongHyun Kim, Moriyama Kiyofumi, Hyun Sun Park, Moo Hwan Kim, and Ho Seon Ahn. Loss of superhydrophobicity of hydrophobic micro/nano structures during condensation. *Scientific Reports*, 5(APRIL):9901, 2015.

[168] Yuhe Shang, Youmin Hou, Miao Yu, and Shuhuai Yao. Modeling and optimization of condensation heat transfer at biphilic interface. *International Journal of Heat and Mass Transfer*, 122:117–127, 2018.

[169] Aref Vandadi, Lei Zhao, and Jiangtao Cheng. Resistant energy analysis of self-pulling process during dropwise condensation on superhydrophobic surfaces. *Nanoscale Advances*, 1(3):1136–1147, 3 2019.

[170] Frank Schellenberger, Jing Xie, Noemí Encinas, Alexandre Hardy, Markus Klapper, Periklis Papadopoulos, Hans Jürgen Butt, and Doris Vollmer. Direct observation of drops on slippery lubricant-infused surfaces. *Soft Matter*, 11(38):7617–7626, 2015.

[171] K. Bellur, E. F. Médici, M. Kulshreshtha, V. Konduru, D. Tyrewala, A. Tamilarasan, J. McQuillen, J. B. Leão, D. S. Hussey, D. L. Jacobson, J. Scherschligt, J. C. Hermanson, C. K. Choi, and J. S. Allen. A new experiment for investigating evaporation and condensation of cryogenic propellants. *Cryogenics*, 74:131–137, 3 2016.

[172] Su Ji Park, Byung Mook Weon, Ji San Lee, Junho Lee, Jinkyung Kim, and Jung Ho Je. Visualization of asymmetric wetting ridges on soft solids with X-ray microscopy. *Nature Communications*, 5(1):1–7, 7 2014.

[173] Cunlong Yu, Longhao Zhang, Yunfei Ru, Ning Li, Chuxin Li, Can Gao, Zhichao Dong, and Lei Jiang. Drop Cargo Transfer via Unidirectional Lubricant Spreading on Peristome-Mimetic Surface. *ACS Nano*, 12(11):11307–11315, 2018.

[174] Dong In Yu, Ho Jae Kwak, Seung Woo Doh, Ho Seon Ahn, Hyun Sun Park, Moriyama Kiyofumi, and Moo Hwan Kim. Dynamics of Contact Line Depinning during Droplet Evaporation Based on Thermodynamics. *Langmuir*, 31(6):1950–1957, 2 2015.